Research Paper

A novel telomere-related genes model for predicting prognosis and treatment responsiveness in diffuse large B-cell lymphoma

Zhijia Zhao[1,*], Xiaochen Shen[2,*], Siqi Zhao[1], Jinhua Wang[1], Yuqin Tian[1], Xiaobo Wang[1], Bo Tang[1]

[1]Department of Hematology, The Second Affiliated Hospital of Dalian Medical University, Dalian 116023, People's Republic of China
[2]Department of Pathology, The Second Affiliated Hospital of Dalian Medical University, Dalian 116023, People's Republic of China
[*]Equal contribution and share first authorship

Correspondence to: Bo Tang, Xiaobo Wang; **email:** bo_tang@126.com, https://orcid.org/0000-0002-0909-3034; dlwangxiaobo@163.com, https://orcid.org/0000-0001-5057-5919
Keywords: diffuse large B-cell lymphoma, telomere-related genes, prognostic model, tumor immune environment, immune checkpoints, drug sensitivity
Received: July 7, 2023 **Accepted:** October 3, 2023 **Published:** November 15, 2023

ABSTRACT

Diffuse large B cell lymphoma (DLBCL) is a highly heterogeneous disease with diverse clinical and molecular features. Telomere maintenance is widely present in tumors, but there is a lack of relevant reports on the role of telomere-related genes (TRGs) in DLBCL. In this study, we used consensus clustering based on TRGs expression to identify two molecular clusters with distinct prognoses and immune cell infiltration. We developed a TRGs scoring model using univariate Cox regression and LASSO regression in the GSE10846 training cohort. DLBCL patients in the high-risk group had a worse prognosis than those in the low-risk group, as revealed by Kaplan-Meier curves. The scoring model was validated in the GSE10846 testing cohort and GSE87371 cohort, respectively. The high-risk group was characterized by elevated infiltration of activated DCs, CD56 dim natural killer cells, myeloid-derived suppressor cells, monocytes, and plasmacytoid DCs, along with reduced infiltration of activated CD4 T cells, Type 2 T helper cells, γδ T cells, NK cells, and neutrophils. Overexpression of immune checkpoints, such as PDCD1, CD274, and LAG3, was observed in the high-risk group. Furthermore, high-risk DLBCL patients exhibited increased sensitivity to bortezomib, rapamycin, AZD6244, and BMS.536924, while low-risk DLBCL patients showed sensitivity to cisplatin and ABT.263. Using RT-qPCR, we found that three protective model genes, namely TCEAL7, EPHA4, and ELOVL4, were down-regulated in DLBCL tissues compared with control tissues. In conclusion, our novel TRGs-based model has great predictive value for the prognosis of DLBCL patients and provides a promising direction for treatment optimization.

INTRODUCTION

Diffuse large B-cell lymphoma (DLBCL), which is the most common subtype of non-Hodgkin's lymphoma, is a highly heterogeneous disease with diverse clinical and molecular features. Based on the cell of origin (COO) of lymphoma cells, DLBCL can be classified into germinal center B-cell (GCB) and activated B-cell (ABC) subgroups [1]. ABC DLBCL patients generally have worse prognosis. It is worth noting that DLBCL patients with similar clinicopathological characteristics have different prognoses [2]. The standard first-line therapy for DLBCL is rituximab plus cyclophosphamide, doxorubicin, vincristine, and prednisone (R-CHOP). Although R-CHOP can achieve long-term remissions in most DLBCL patients, 30–40% of them experience relapse with poor prognoses [3]. Various strategies have been explored to improve the efficacy of the standard

regimen, including dose intensification, novel therapeutic agents, and next-generation anti-CD20 antibodies [4–6]. However, these approaches have not yielded significant clinical benefits [7]. Therefore, early prognosis evaluation and optimization of therapeutic options are crucial for improving the survival outcomes of DLBCL patients. The international prognostic index (IPI) is currently a widely used clinical tool for predicting the prognosis of DLBCL patients [8]. However, it has a weakness in effectively identifying prognosis of DLBCL patients with very poor survival. As the IPI score only provides prognostic information based on clinical variables, a gene expression-based signature may be a valuable supplement for further assessing the prognosis of DLBCL.

In the process of genome replication in most organisms, the main mechanism of telomere length maintenance is the completion of DNA telomere repeats by telomerase [9]. Telomerase is a ribonucleoprotein complex composed of ribonucleic acid (RNA) and protein. Its core dimer consists of telomerase reverse transcriptase (TERT) and telomerase RNA component (TERC), which is used as a template for RNA-dependent DNA synthesis [10]. Telomere maintenance is widely present in tumors and plays an important role in extending telomere length, among which telomerase activity and alternative length of telomeres (ALT) pathway are the main pathways for telomere maintenance. Among these two pathways, telomerase activation is more common and has been reported in almost all types of tumors [11, 12]. In lymphoma, Lima et al. reported that Hodgkin lymphoma (HL) cells are most likely to have telomerase activation pathways that extend telomeres, followed by the ALT pathway [13]. But there are no relevant reports in DLBCL. There are five main treatment methods for telomerase inhibition currently, including anti-hTR of oligonucleotides, nucleoside analogue, human telomerase (hTERT) small molecule inhibitor, immunotherapy for hTERT and G4 stable ligand. GRN163L (Imetelstat), one of anti-hTR of oligonucleotides, has been proven to have clinical efficacy in treating myelofibrosis and low-risk myelodysplastic syndromes [14]. Because telomeres have length abnormalities in most tumor types including lymphoma, and telomerase inhibition is currently a clear treatment method. Therefore, telomere-related genes (TRGs) should also have potential functions, prognostic judgments, therapeutic targets, and other values in DLBCL.

In this study, we comprehensively analyze the prognostic values of TRGs. Our analysis identified two distinct molecular subgroups based on expression patterns of TRGs. Notably, we developed and validated the first risk model based on TRGs in DLBCL, which demonstrated excellent predictive ability for the prognosis of DLBCL patients. By RT-qPCR, we further validated expression of candidate genes of the TRGs model, and found three of them, TCEAL7, EPHA4 and ELOVL4, were significantly lower in the DLBCL lymph node tissues and cell lines compared with normal lymph node tissues. Furthermore, we investigated the relationship between the immune infiltration, immune checkpoints and TRGs risk score, and further predicted several chemotherapy drugs that may be effective in high or low-risk DLBCL patients.

METHODS

Data acquisition

In this study, we obtained the mRNA expression profile and corresponding clinical information from the Gene Expression Omnibus (GEO) database. To minimize survival bias, we selected samples with a survival time greater than 0 and complete survival status information. Using this criterion, we extracted 414 samples from the GSE10846 dataset and 221 samples from the GSE87371 dataset. Additionally, we randomly divided the 414 samples in the GSE10846 dataset into a training cohort and a testing cohort at a 7:3 ratio. We used the testing cohort in the GSE10846 dataset as an internal validation cohort, and the GSE87371 dataset as an external validation cohort to verify the predictive ability of the TRG risk model. The TRGs were obtained from Telnet (http://www.cancertelsys.org/telnet/) [15], which maintains a list of genes that have been reported to be involved in telomere maintenance.

Construction and validation of a TRGs scoring model

In this study, we utilized univariate Cox regression analysis via the R package "survival" to identify prognostic TRGs in the GSE10846 dataset. DLBCL patients were divided into 2 clusters based on different expression patterns of TRGs via the "ConsensusClusterPlus" R package. Thirty differentially expressed prognostic TRGs were found between clusters 1 and 2, and we then used the least absolute shrinkage and selection operator (LASSO) regression in the training cohort to develop a prognostic risk scoring model based on 7 TRGs. The risk scores were calculated using a formula, risk score = Σ(Expi × Coefi). We calculated risk scores in all DLBCL patients. Based on the median risk score, we divided the training cohort into low-risk and high-risk groups. We performed principal component analysis (PCA) using the "stats" package in R to explore the internal relationship between the two groups. We used Kaplan-Meier (K-M) curves to analyze overall survival (OS). To evaluate the accuracy and reliability of the risk

scoring signature, time-dependent receiver operating characteristic (ROC) curve analysis was generated using the "TimeROC" package in R.

Sample information and DLBCL cell lines

The collection of tissue samples for this study was approved by the Human Ethics Committee of the Second Hospital of Dalian Medical University, and all patients provided informed consent. We obtained nine lymph node samples from different patients at the Second Affiliated Hospital of Dalian Medical University, including two DLBCL-invaded lymph nodes from DLBCL patients and seven normal lymph nodes from abandoned tissues after surgery. Additionally, DLBCL cell lines HBL-1 and OCI-LY10 were acquired from Professor Li Li at the Second Affiliated Hospital of Dalian Medical University. HBL-1 cells were cultured in RPMI-1640 medium supplemented with 10% fetal bovine serum and 1% penicillin-streptomycin solution at 37°C with 5% CO_2. OCI-LY10 cells were cultured in IMDM medium supplemented with 20% fetal bovine serum and 1% penicillin-streptomycin solution in a 37°C incubator with 5% CO_2.

Quantitative real-time PCR (RT-qPCR)

Total RNA was extracted from DLBCL cell lines or lymph node samples using Trizol reagent. Reverse transcription was performed using the PrimeScriptTMRT reagent Kit with gDNA Eraser (Takara, Japan) and RT-qPCR was performed using TB Green Premix Ex Taq™ II (Takara), according to the respective manufacturer's instructions. The expression levels of target genes were normalized against the ACTB expression level and presented as $2^{-\Delta Ct}$. The primer sequences for RT-PCR were designed using Primer Premier 5 software and verified on BLAST websites. The primer sequences are provided in Supplementary Table 1.

Clinical correlations and independent prognosis value of the TRGs score

The TRG scores in different clinical and pathological feature groups were performed via Wilcoxon signed-rank test and Chi-square test in the GSE10846 training dataset. Univariate and multivariate Cox regression via R package "survival" was used to evaluate the independent prognostic value of the risk score and other clinicopathological features.

Nomogram construction

SPSS Statistics 17.0 was applied for the evaluation of collinearity and the correlation analysis of variables. Variables with strong correlations ($r > |0.7|$) were excluded from the subsequent analysis [16, 17]. The package "rms" of R language was applied to generate a nomogram. Area under the curve (AUC) of ROC curves was calculated using the package "survivalROC" of R language. Then, difference analysis between the AUCs of the nomogram and IPI score was conducted using Delong test via MedCalc software 20.027 for the evaluation of the nomogram's prognostic ability and reliability [18]. In addition, decision curve analysis (DCA) was conducted, and the nomogram's clinical utility was evaluated according to net benefits under the condition of different risk thresholds.

Immune analyses

The single-sample Gene Set Enrichment Analysis (ssGSEA) was used to assess the enrichment of 28 immune cells and 38 immune checkpoints in the DLBCL samples, no matter between the two clusters based on differential expression patterns of TRGs, or between the high- and low-risk groups in the GSE10846 training cohort.

Prediction of chemosensitivity

We predicted the IC50 of chemotherapeutic sensitivity for the high-risk group and low-risk group via the R package "pRRophetic".

Data availability statement

The datasets generated and/or analyzed during the current study are available in the GEO dataset (https://www.ncbi.nlm.nih.gov/geo/).

RESULTS

Molecular clustering based on the TRGs in DLBCL

Initially, we retrieved 2086 TRGs from TelNet. Using univariate Cox proportional hazards regression analysis, we identified 816 prognostic TRGs that were significantly associated with the OS of DLBCL in the GSE10846 dataset (Supplementary Table 2, $p < 0.05$). Based on the expression patterns of these 816 prognostic TRGs, we performed consensus clustering to classify 414 DLBCL patients in the GSE10846 dataset into different molecular subgroups. Consensus clustering was most suitable when k = 2, as we increased the number of clusters (k) from 2 to 5 (Figure 1A, 1B and Supplementary Figure 1). Subsequently, we obtained two distinct clusters, with 181 patients in cluster 1 and 233 patients in cluster 2. K-M curves revealed that DLBCL patients in cluster 1 had significantly worse OS compared to those in

cluster 2 (Figure 1C, $p < 0.001$). A heatmap illustrated 65 differentially expressed genes (DEGs) in 2086 TRGs between clusters 1 and 2 (Figure 1D).

Moreover, we investigated the differences in immune cell infiltration between these two subgroups. As depicted in Supplementary Figure 2A, activated B cells, activated CD8 T cells, activated dendritic cells (DCs), CD56 dim natural killer (NK) cells, myeloid-derived suppressor cells (MDSCs), and plasmacytoid DCs in cluster 1 exhibited higher infiltration levels than those in cluster 2. Conversely, activated CD4 T cells, gamma delta T cells, macrophages, mast cells, NK cells, neutrophils, regulatory T cells, type 17 T helper cells,

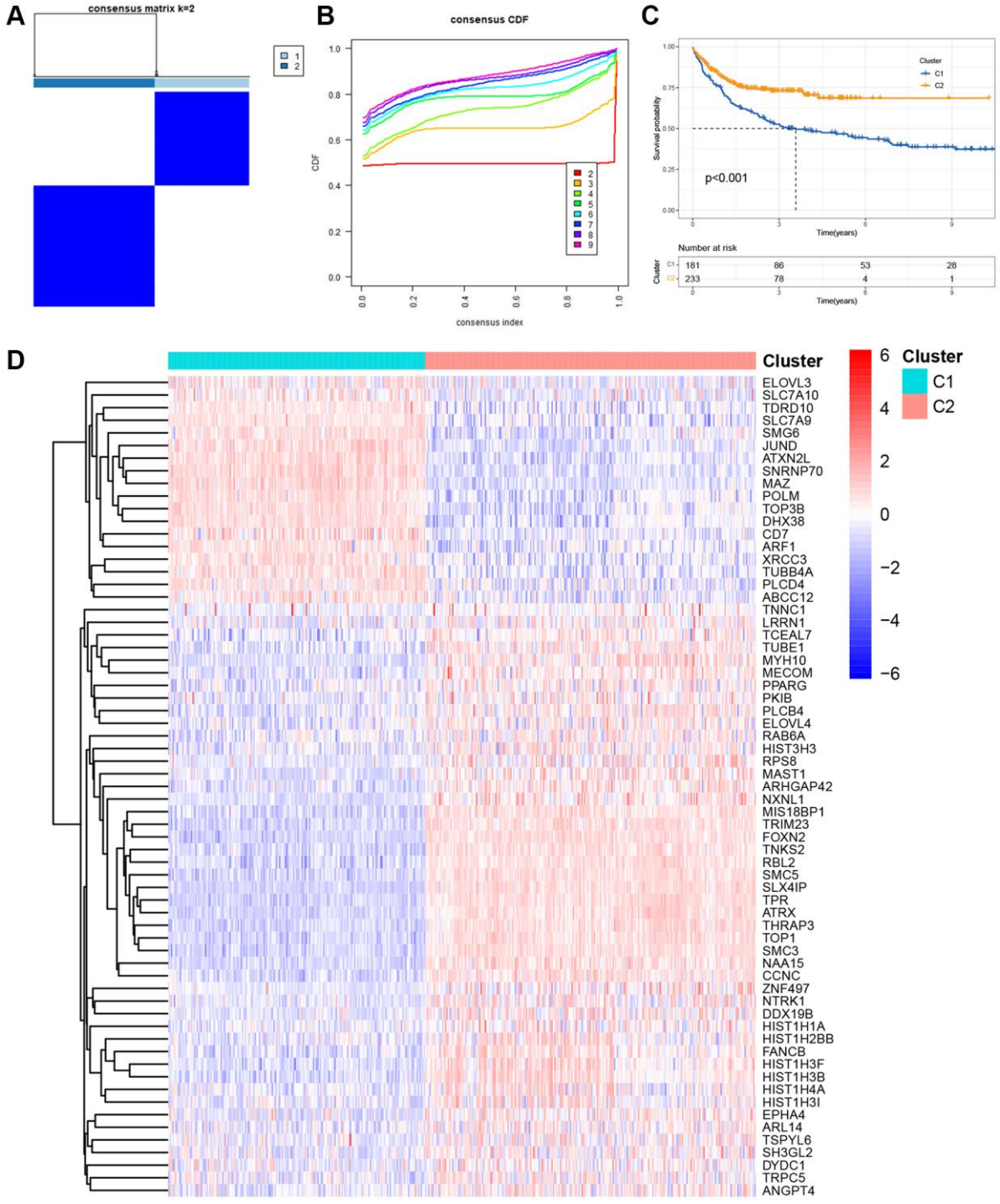

Figure 1. Molecular clustering based on the TRGs in DLBCL. (**A**) The consensus matrix by cluster analysis based on TRGs. Two clusters (k = 2) would be best. (**B**) Consensus clustering CDF with *k* value 2 in GSE10846 dataset. (**C**) Kaplan-Meier curves of OS in two clusters. (**D**) Heatmap of 65 differentially expressed genes in TRGs between clusters 1 and 2.

type 2 T helper cells, central memory CD4 T cells, central memory CD8 T cells, and effector memory CD8 T cells in cluster 1 displayed lower infiltration levels than those in cluster 2. Additionally, we explored 38 immune checkpoint molecules between these two clusters and observed that several crucial immune checkpoint molecules, such as CD274 and PDCD1, were over-expressed in cluster 1 (Supplementary Figure 2B).

Construction of a prognosis-associated scoring model composed of 7 TRGs

Given the prognostic value of TRG expression patterns in DLBCL, we developed a TRG-based scoring model using differentially expressed TRGs between two distinct clusters. We randomly divided 414 DLBCL patients from GSE10846 into a training cohort (n = 292) and a testing cohort (n = 122) in a 7:3 ratio. The above 65 differentially expressed TRGs between clusters 1 and 2 were used to perform univariable Cox regression analysis and identify 30 TRGs associated with OS in the GSE10846 training cohort ($p < 0.05$). To avoid overfitting, we conducted LASSO regression analysis on the 30 TRGs and selected seven genes for the scoring model based on the optimal value of λ (Figure 2A, 2B). Among these genes, TUBB4A, PPARG, and ELOVL3 were identified as risk genes with HR > 1, while TCEAL7, EPHA4, ELOVL4, and ARL14 were identified as protective genes with HR < 1 (Table 1). The risk scores were calculated using the formula: risk score = (0.1873 × Exp TUBB4A) + (−0.1179 × Exp TCEAL7) + (0.2908 × Exp PPARG) + (−0.1075 × Exp EPHA4) + (−0.1001 × Exp ELOVL4) + (0.1023 × Exp ELOVL3) + (−0.0735 × Exp ARL14). Using the median risk score, we categorized DLBCL patients in the GSE10846 training cohort into high- and low-risk groups. The scatter plot revealed a worse survival outcome in the high-risk group compared to the low-risk group (Figure 2C). PCA showed a significant distribution of DLBCL patients in the high-risk and low-risk groups between two trends (Figure 2D). Furthermore, K-M curves demonstrated that DLBCL patients in the high-risk group had significantly worse OS, as illustrated in Figure 2E. We then evaluated the TRGs scoring model's predictive efficiency using time-dependent ROC analysis, and the AUC reached 0.688 at 1-year, 0.720 at 3-year, and 0.718 at 5-year (Figure 2F).

Validation of the TRGs-based scoring model

To evaluate the prediction performance and robustness of the risk model, we used the GSE10846 testing cohort as an internal validation cohort and the GSE87371 dataset as an external validation cohort. Using the same formula, we divided the patients into low- and high-risk groups based on their median risk scores in these validation cohorts. The scatter plots further revealed that patients in the high-risk group had a higher possibility of early death than patients in the low-score group in the GSE10846 testing cohort and GSE87371 cohort, respectively (Figure 3A, 3B). PCA showed that DLBCL patients in high- and low-risk groups were well-separated in validation cohorts (Figure 3C, 3D). K-M curves revealed that DLBCL patients in the low-risk group had a better prognosis than those in the high-risk group, respectively (Figure 3E, 3F). The AUC at 1-, 3-, and 5-year in the GSE10846 testing cohort were 0.655, 0.639, and 0.638 respectively (Figure 3G). In the GSE87371 cohort, the AUC reached 0.628 at 1-year, 0.655 at 3-year, and 0.714 at 5-year (Figure 3H). Overall, our prognostic TRGs-based scoring model demonstrated effective predictive efficiency in the prognosis of DLBCL patients.

Expression evaluation of candidate TRGs in the model

To validate the expression of 7 candidate model genes in DLBCL patients, we collected samples from two DLBCL cell lines (HBL-1 and OCI-LY10), two DLBCL-invaded lymph nodes, and seven normal lymph nodes. RT-qPCR analysis revealed that the expression levels of several protective genes, TCEAL7, EPHA4, and ELOVL4, were significantly lower in the DLBCL group than in the control group (Figure 4A–4J). There was no statistically significant difference in the expression of the other four candidate genes between the DLBCL and control groups based on the current sample sizes (Supplementary Figure 3).

Clinical correlations and independent prognosis value of TRGs risk model

To evaluate the clinical significance of the TRGs risk score, we compared the risk scores between different subgroups based on clinical features in the GSE10846 training cohort. As shown in Figure 5A–5C, the risk scores were significantly higher in DLBCL patients with ECOG ≥ 2, stage 3–4, or ABC subtype.

To explore whether TRG risk score could be an independent prognostic factor, we first used univariate Cox regression analysis to evaluate it and other clinical characteristics (age, gender and stage) in these cohorts. Age, stage and TRGs risk score were related to the OS of DLBCL patients in the GSE10846 training cohort (all p-values < 0.001, Figure 5D). In the GSE10846 testing cohort, age and TRGs risk score were highly associated with the prognosis of DLBCL patients (all p-values < 0.05, Supplementary Figure 4A). In the GSE87371

cohort, age, stage and TRGs risk score had close relationships with OS (all p-values < 0.001, Supplementary Figure 4B). Furthermore, we conducted multivariate Cox regression analysis to adjust for confounding factors. TRG risk score was found to be an independent predictor of OS in all of the 3 cohorts (Figure 5E and Supplementary Figure 5A, 5B; GSE10846 training cohort: HR = 2.060, p < 0.001; GSE10846 testing cohort: HR = 1.740, p = 0.036; GSE87371 cohort: HR = 4.359, p = 0.014).

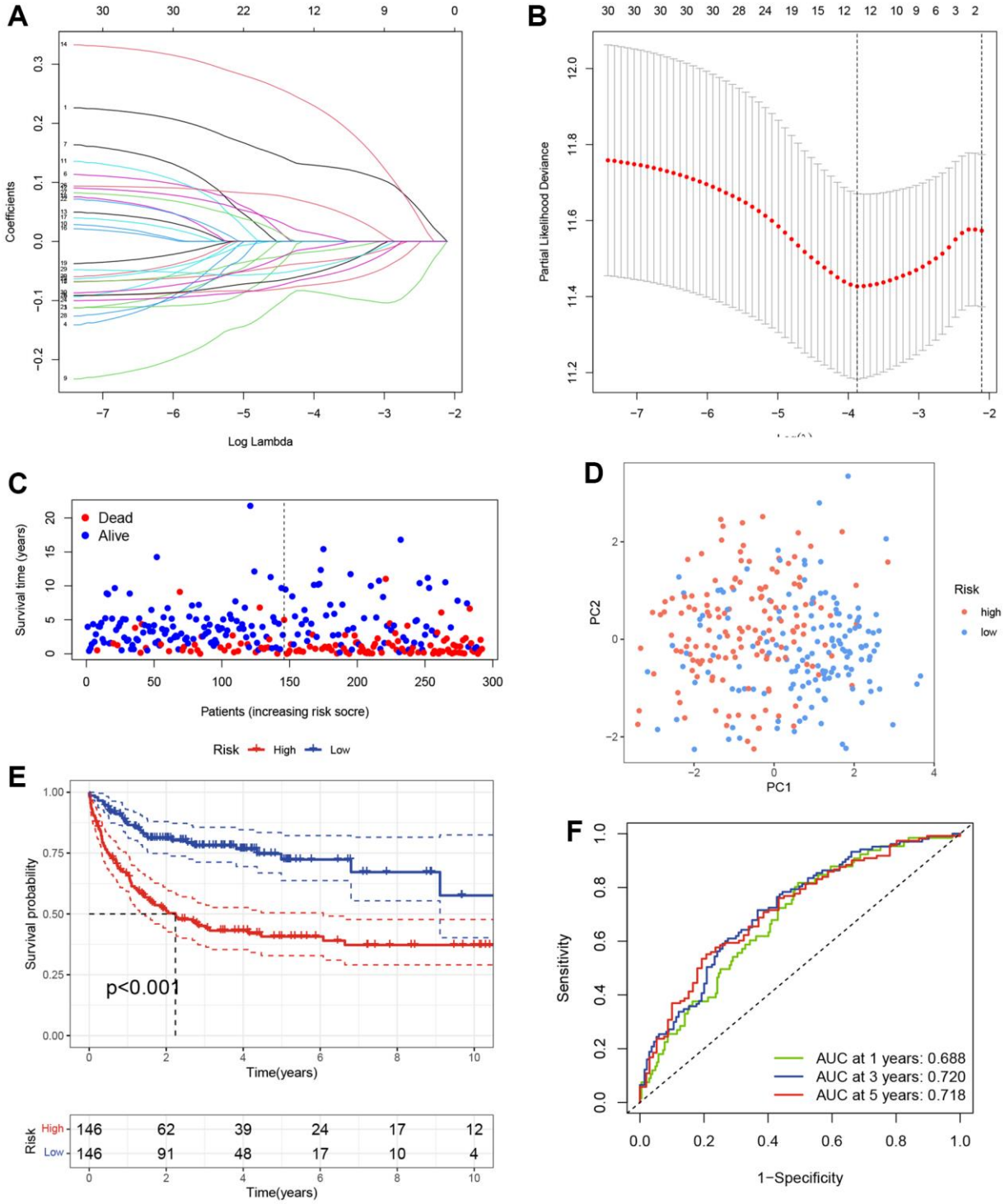

Figure 2. Construction of the TRGs-based scoring model. (**A**) LASSO coefficient profiles of TRGs in GSE10846 training cohort. (**B**) Selection of the optimal parameter (λ) in the LASSO model. (**C**) Survival status of DLBCL patients in GSE10846 training cohort. (**D**) PCA analysis of the DLBCL patients based on the TRGs score in GSE10846 training cohort. (**E**) Kaplan-Meier curves of OS based on TRGs score in GSE10846 training cohort. (**F**) Time-dependent ROC analysis of the TRGs score in GSE10846 training cohort.

Table 1. LASSO coefficient, *p*-values and hazard ratios of the seven TRGs.

Genes	Coef	HR	HR.95L	HR.95H	*P*-value
TUBB4A	0.187368	1.206071	1.029736	1.412602	0.020162
TCEAL7	−0.11791	0.888775	0.791086	0.998527	0.04717
PPARG	0.290805	1.337503	1.179622	1.516516	5.69E-06
EPHA4	−0.10755	0.898033	0.781636	1.031763	0.128894
ELOVL4	−0.1001	0.904749	0.806728	1.01468	0.087103
ELOVL3	0.10239	1.107815	0.970687	1.264315	0.128841
ARL14	−0.07354	0.929102	0.843152	1.023814	0.137605

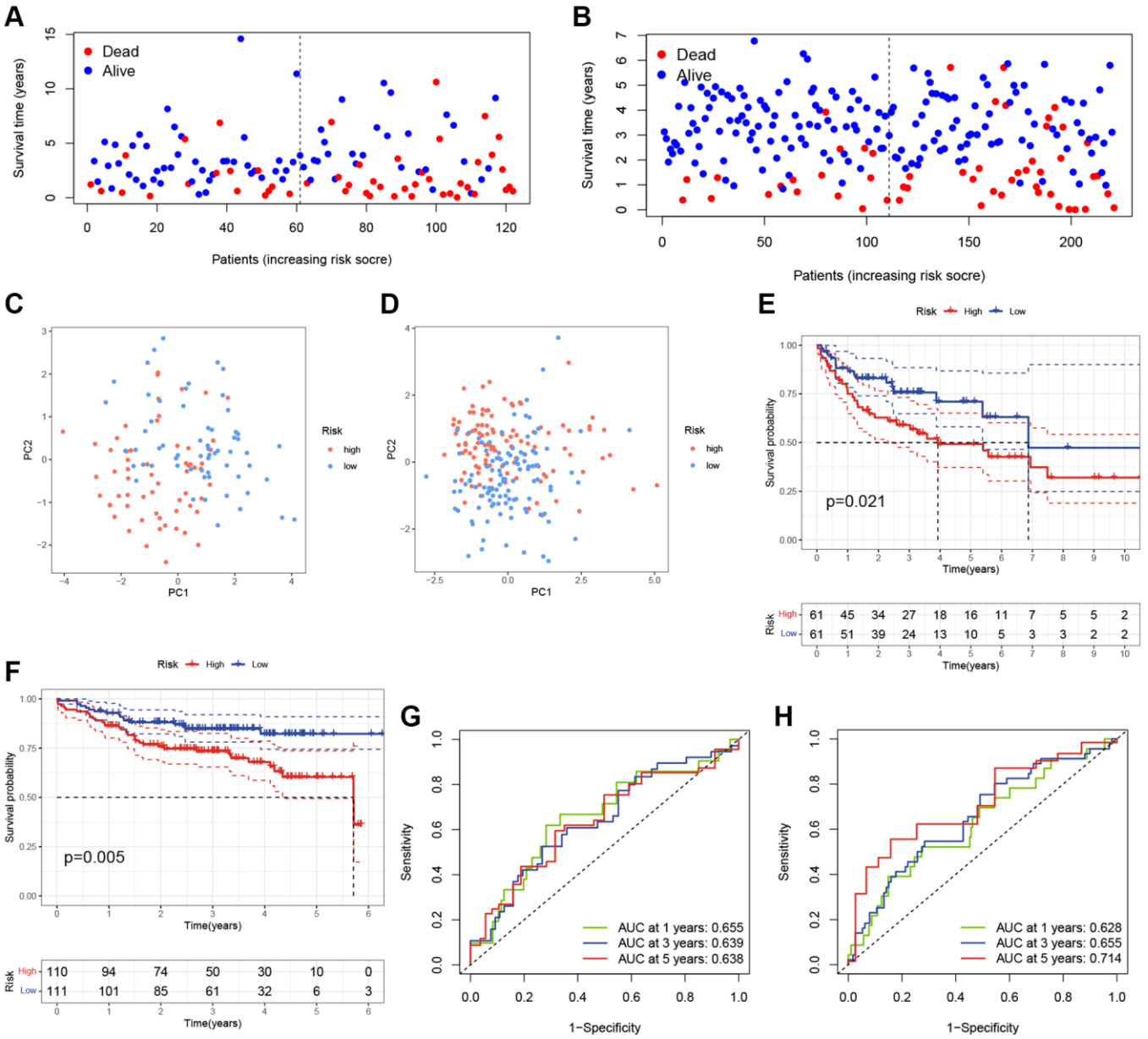

Figure 3. Validation of the TRGs-based scoring model. (**A**, **B**) The survival statuses of DLBCL patients in (**A**) GSE10846 testing cohort and (**B**) GSE87371 cohort. (**C**, **D**) The PCA of DLBCL patients in (**C**) GSE10846 testing cohort and (**D**) GSE87371 cohort. (**E**, **F**) Kaplan-Meier curves of OS based on TRGs score in (**E**) GSE10846 testing cohort and (**F**) GSE87371 cohort. (**G**, **H**) Time-dependent ROC analyses of the ARG score in (**G**) GSE10846 testing cohort and (**H**) GSE87371 cohort.

Nomogram construction

Nomograms are useful tools for predicting patient prognosis and can assist with clinical decision-making. After the evaluation of collinearity and the correlation analysis of variables (Supplementary Tables 3 and 4), we constructed a prognostic nomogram based on the TRGs risk score and clinical features, including age,

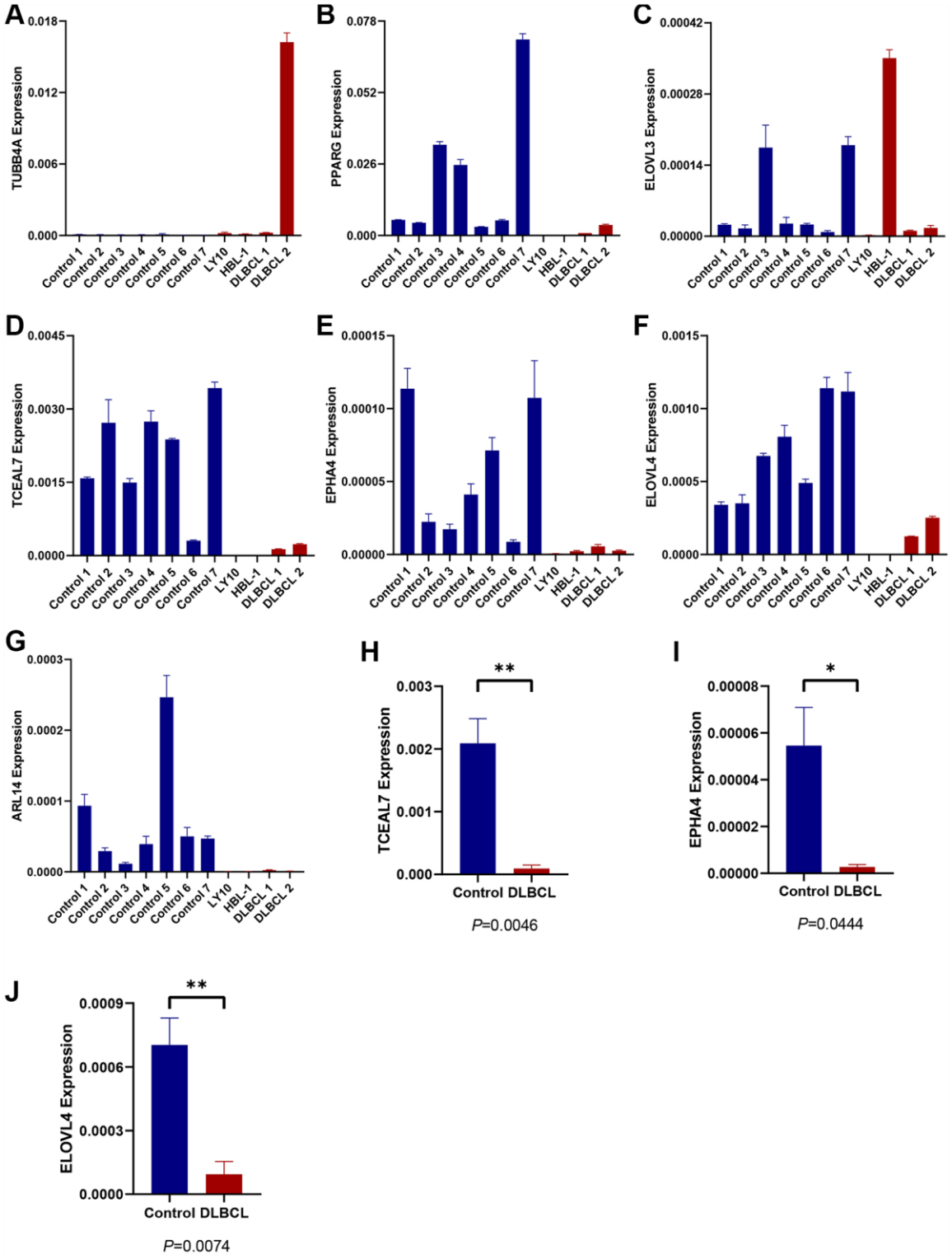

Figure 4. Expression evaluation of candidate TRGs in the model. (**A**–**G**) The expression level of 7 TRGs in two DLBCL cell lines (HBL-1 and OCI-LY10), two DLBCL-invaded lymph node samples (DLBCL 1 and DLBCL 2) and seven normal lymph node samples (control 1–7), respectively. (**H**, **I**) The expression of (**H**) TCEAL7, (**I**) EPHA4, and (**J**) ELOVL4 in DLBCL group and control group.

ECOG, LDH level, number of extranodal sites and IPI score (Figure 6A). The nomogram showed excellent consistency between predicted and observed OS at 1-year, 3-year, and 5-year, as demonstrated by the favorable match of the calibration curves (Figure 6B). We further compared the ROC curves of the nomogram with the IPI score and found that the AUC of the nomogram was higher than that of the IPI score at 2- and 5-year survival outcome (2-year 0.815 vs. 0.758 and 5-year 0.846 vs. 0.777, Figure 6C, 6D). Subsequently, difference analysis (Table 2) presented statistical differences between the AUCs of nomogram and IPI score at 2- and 5-year survival. Meanwhile, DCA curves were made for the comparations of predicted net benefit between the nomogram and IPI score, and the findings reflected the certain feasibility of this constructed for making valuable prognostic judgments and therapeutic guidance. As shown in Figure 6E, 6F, when the risk threshold of patients was approximately 15–55% at 2-year survival or 20–65% at 5-year survival predicted by the nomogram, the nomogram application for therapeutic guidance would provide more benefit than either treating all patients or employing no treatment. Additionally, DCA curves showed that the nomogram presented superior benefits compared with IPI score in the condition of 15–35% threshold probability at 2-year survival or 20–45% threshold probability at 5-year survival. These results demonstrate that the nomogram has better ability to forecast the OS of DLBCL than the IPI score.

Correlation between risk score and immune microenvironment

The tumor immune microenvironment plays a crucial role in the therapeutic response and prognosis of tumors. Therefore, we analyzed the immune infiltration of high- and low-risk groups in the GSE10846 training cohort. The ssGSEA revealed higher levels of infiltrating activated DCs, CD56 dim NK cells, MDSC, monocytes, and plasmacytoid DCs in the high-risk group. Additionally, lower levels of infiltrating activated CD4 T cells, Type 2 T helper cells, γδ T cells, NK cells, and neutrophils were observed in the high-risk group (Figure 7A). Furthermore, expression differences in most of the immune checkpoints were found between

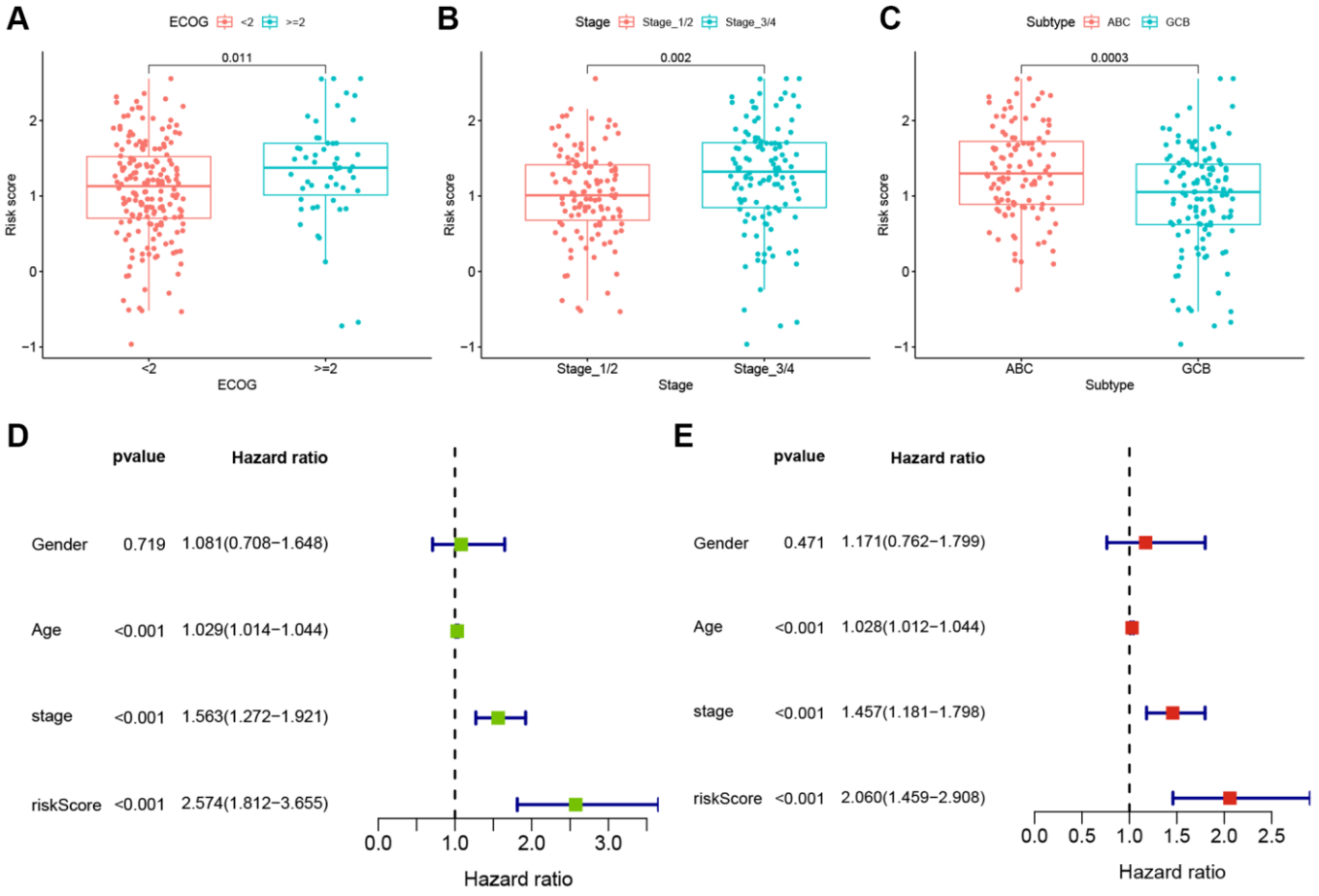

Figure 5. Clinical correlations and independent prognosis value of TRGs risk model. (**A**–**C**) TRGs risk scores in different DLBCL subgroups of (**A**) EOCG, (**B**) stage and (**C**) subtype. (**D**) Univariate Cox regression analysis of TRGs score and clinical features in GSE10846 training cohort. (**E**) Multivariate Cox regression analysis of TRGs score and clinical features in GSE10846 training cohort.

Table 2. Difference analysis of AUCs between the nomogram and IPI.

	2-year survival	5-year survival
Difference between AUCs	0.057	0.0691
z statistic	2.211	2.444
p-value	0.0270	0.0145

the high-risk and low-risk groups. Higher expression levels of PDCD1, CD274, LAG3, FGL1, LGALS9, PVR, TNFRSF18, TNFSF18, YTHDF1, IL12A, and TNFSF9 were observed in the high-risk compared to the low-risk group. Conversely, expression of B2M, CD40LG, CD86, ICOS, IL23A, JAK1, JAK2, LDHA, PTPRC, SIGLEC15, and TNFRSF9 were down-regulated in the high-risk group (Figure 7B).

The risk signature predicted the sensitivity of novel chemotherapy

We estimated the IC50 values of different drugs in the GSE10846 dataset to explore whether the TRG score presented a potential association with drug sensitivity. Compared to the low-risk group, the high-risk group exhibited increased sensitivity to bortezomib,

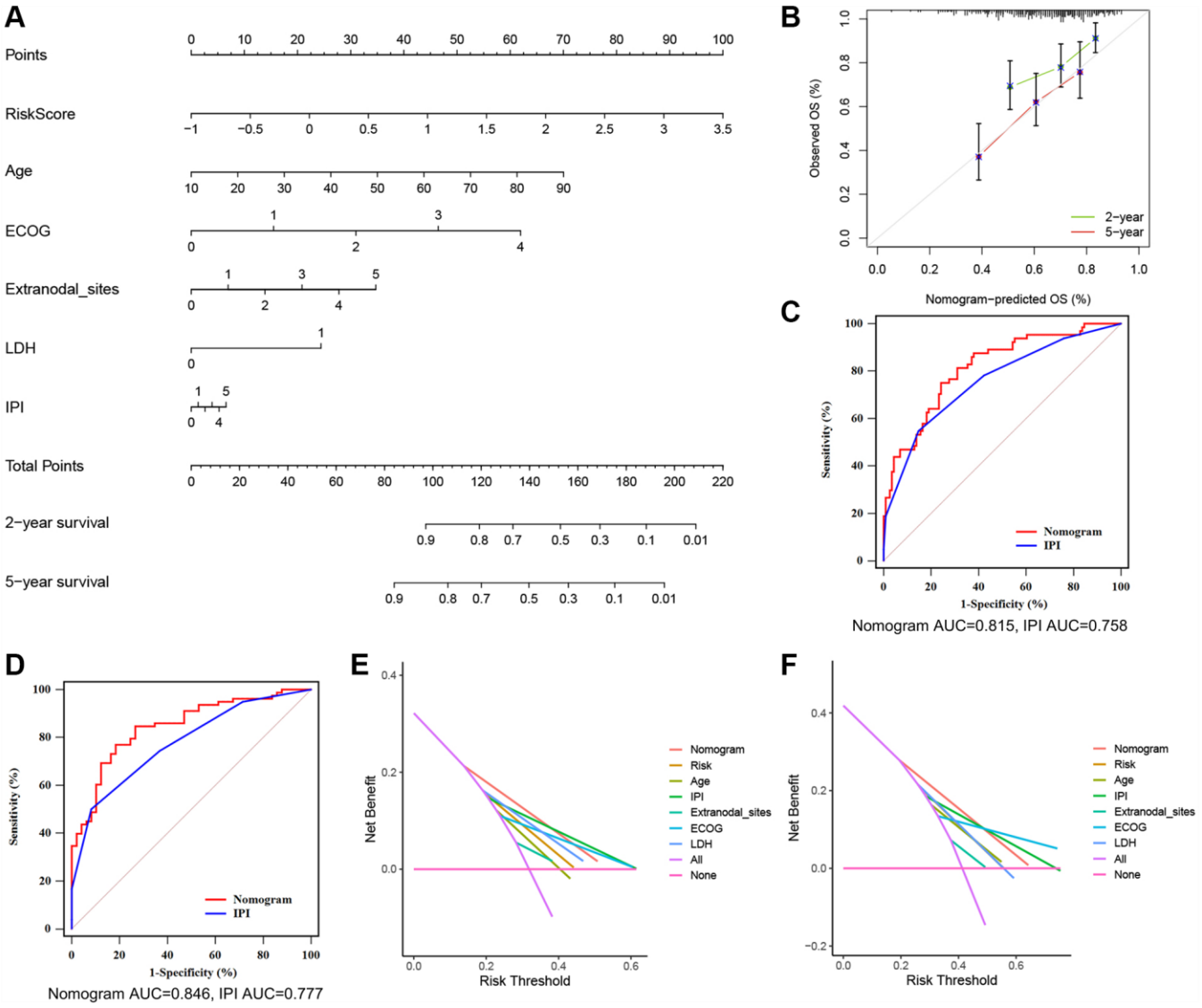

Figure 6. A nomogram based on the TRGs risk score, IPI score and clinical features. (**A**) A nomogram for the prediction of DLBCL patients' 2- and 5-year survival probability according to the TRGs score, IPI score and clinical factors. (**B**) Nomogram-predicted percentages and the observed probabilities of 2- and 5-year survival. (**C**, **D**) Time-dependent ROC analysis of the nomogram and IPI score at 2- (**C**) and 5-year (**D**) survival. (**E**, **F**) DCA of the constructed nomogram compared with different indicators at 2- (**E**) and 5-year (**F**) survival.

rapamycin, AZD6244 (MEK1/2 inhibitor), and BMS.536924 (IGF-1R inhibitor) (Figure 8A). DLBCL patients in the low-risk group showed sensitivity to cisplatin (a drug used in several DLBCL second-line chemotherapy regimens) and ABT.263 (Bcl-2 inhibitor, Figure 8B).

DISCUSSION

Chemotherapy and immunotherapy have played principal roles in the treatment of DLBCL patients, but the overall survival rate of DLBCL remains disappointing due to phenotypic heterogeneity and high

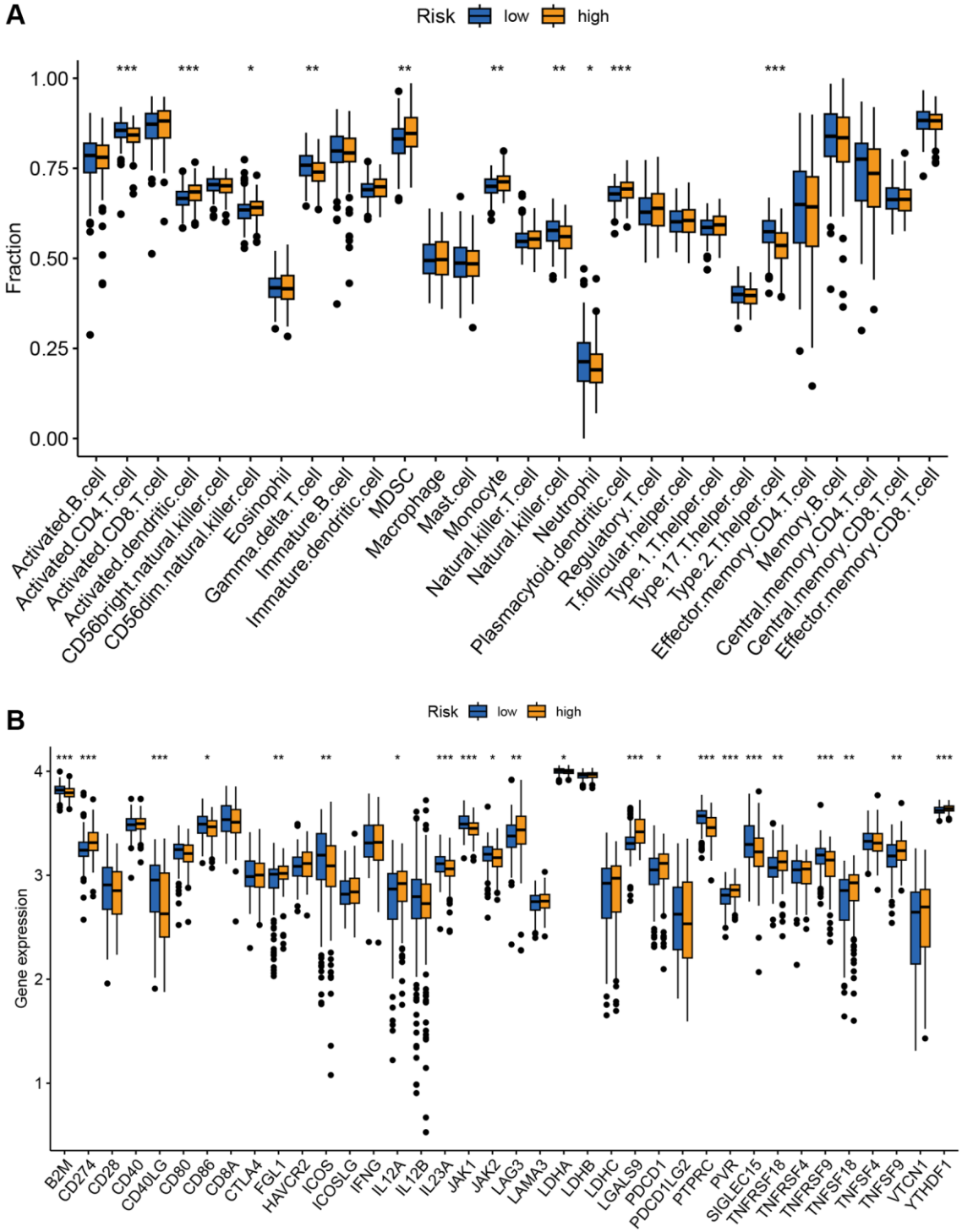

Figure 7. Correlation analysis of TRGs risk score with immune landscape. (**A**) The proportion of 28 immune cells between low-risk and high-risk groups ($^{*}p < 0.05$; $^{**}p < 0.01$; and $^{***}p < 0.001$). (**B**) The distribution of 38 immune checkpoints between the high-risk and low-risk groups ($^{*}p < 0.05$; $^{**}p < 0.01$; and $^{***}p < 0.001$).

relapse rate. Dividing patients into high-risk or low-risk groups to evaluate prognosis and drug reaction can help doctors increase accuracy and personalize clinical treatment. Telomere maintenance is widely present in tumors and plays an important role in extending telomere length, which can lead to immortalization and uncontrolled proliferation [19]. However, the relationship between TRGs and prognosis of DLBCL is rarely reported. Furthermore, there has been no report about TRG-based scoring model in DLBCL available.

To the best of our knowledge, our study is the first to investigate the correlation between TRGs and the prognosis of DLBCL. Using consensus clustering, we identified two subtypes with significant differences in prognosis. Compared to cluster 2, the prognosis of DLBCL patients in cluster 1 was poor. Because expression patterns of TRGs can effectively distinguish the prognosis of DLBCL patients, we further construct a prognostic TRGs scoring model. Among the candidate model genes, TUBB4A, PPARG and ELOVL3 served as risk genes with HR > 1, and TCEAL7, EPHA4, ELOVL4 and ARL14 were protective genes with HR < 1.

Previous studies have expounded the specific roles of the candidate TRGs in different tumors. As one hot spot of the current research, PPARG encodes PPARγ, one of representative nuclear receptors. PPARγ is related to the pathology of many diseases, including obesity, diabetes, atherosclerosis and cancer, and notably, the effects of PPARγ in the tumor occurrence and development are not unifying [20]. PPARγ functions as a tumor-suppressive factor via PPARγ/RXRα signaling pathway in several tumor types [21]. Contrarily, it has been reported that the activation of PPARγ/RXRα induces the microenvironmental reprogramming in the bladder cancer, which is beneficial to the tumorigenesis [22]. In addition to those solid tumors, the function of PPARG has been also studied in lymphoma. As one of oxidative stress genes, PPARG increases the generation of reactive oxygen species appears to increase the risk for non-Hodgkin lymphoma, particularly DLBCL [23]. Elevated expression of PPARγ increases expression of fatty acids to inhibit NK cell response and cell metabolism in invasive B-cell lymphoma, which leads to the functional adaptation of NK cells to fatty acid rich lymphoma [24]. EPHA4 belongs to the largest

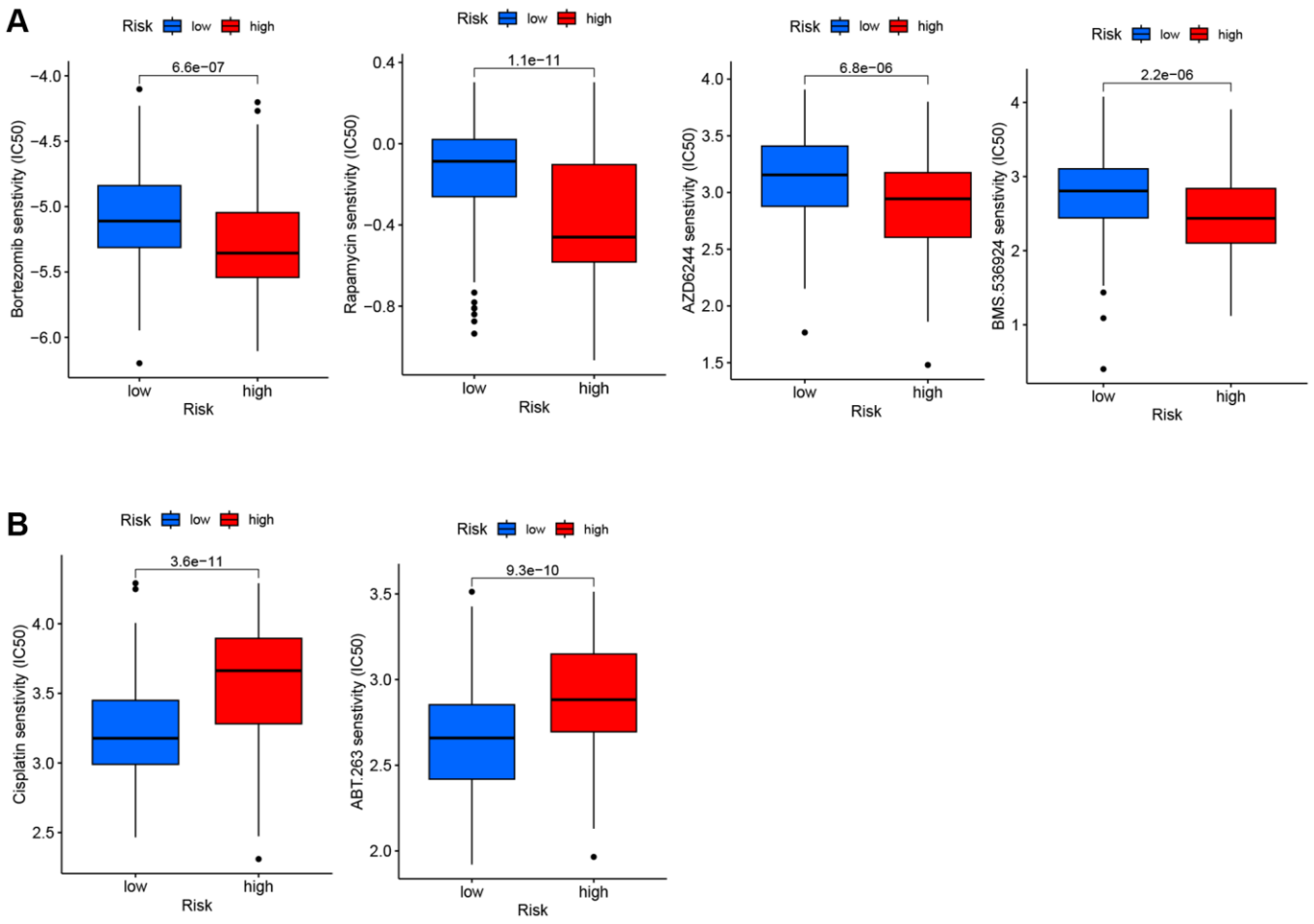

Figure 8. IC50 of six drugs between low-risk and high-risk groups. (**A**) The high-risk group exhibited more sensitivity to the four drugs compared to the low-risk group. (**B**) The high-risk group exhibited less sensitivity to the two drugs compared to the low-risk group.

RTK-Eph family. Some studies have shown that RTKs play an important role in Epstein-Barr virus (EBV)-related tumor formation, because deceased expression of EPHA4 is associated with EBV infection. EBV is an important pathogenic factor for lymphoma and is closely related to the pathogenesis of some DLBCL [25]. Virus-related lymphoid malignancies activate telomerase early via the exogenous regulator of hTERT [26]. These findings seem to indicate that reduced expression of EPHA4 may cause lymphoma through EBV infection. Corresponding to the above findings, overexpression of EPHA4 prevented proliferation of lymphoblastoid cell lines [27]. According to the scoring TRGs model we constructed, EPHA4 was identified as a protective gene and its low-expression was related to poor survival in DLBCL. In the combination of low EPHA4 expression confirmed via RT-qPCR, the tumor-preventing role and prognostic value of EPHA4 in DLBCL become more convincing. Besides, EPHA4 may be applied in the molecular diagnosis of Sézary syndrome-related cutaneous T-cell lymphomas, and the membrane-bound EPHA4 receptor can serve as a target for targeted therapeutic interventions [28]. Among other five TRGs, TUBB4A serves as a tumor-promoting factor in several tumor types including melanoma and prostate cancer, and ELOVL3 is considered as a risk gene in hepatocellular carcinoma [22, 29, 30]. However, there has been no relevant report in lymphomas. Moreover, TCEAL7 is a competitive inhibitor of c-Myc, and c-Myc plays an important role in telomere maintenance mechanisms as a hTERT transcriptional activator [31, 32]. Studies show that TCEAL7 is down-regulated in many tumors, and is considered as a putative tumor suppressor gene. Consistent with the conclusions made by others, TUBB4A and ELOVL3 presented as risk genes, while down-regulation of TCEAL7 was confirmed in DLBCL and correlated with poor prognosis in our study. As for ELOVL4, the effects in tumors remain controversial. It has been reported that ELOVL4 serves as a tumor suppressor via the NOTCH-RIPK4-IRF6-ELOVL4 axis in squamous cell carcinoma, and its overexpression is related to the good prognosis for neuroblastoma patients [33, 34]. On the contrary, ELOVL4 is identified as a risk gene in gastric cancer [35]. Moreover, ARL14 has only been reported in non small-cell lung cancer (NSCLC), and increased expression of ARL14 was significantly correlated with poor survival [36]. However, ARL14 was considered as a protective gene in our study, differing from the function observed in NSCLC. We considered that the difference may be related to the variations of tumor tissue origins and tumor microenvironment (TME). Therefore, more experimental evidence is still needed to identify the respective functions of these TRGs in DLBCL.

TRG risk model was not only validated in the training dataset, but also in the external validation set. The AUC values of the ROC curves in our training dataset for 1-, 3-, and 5-year OS were 0.688, 0.720, and 0.718, 1-, 3-, and 5-year OS were 0.655, 0.639 and 0.638 in internal validation set, and 1-, 3-, and 5-year OS were 0.628, 0.655 and 0.714 in external validation set, respectively. These results indicate that TRG risk model is a stable and reliable model for evaluating the prognosis of DLBCL. A nomogram that integrates TRG risk score, IPI score and other clinical features such as age, ECOG status, extranodal sites, and LDH level further provides the possibility of individualized utility in predicting patient prognosis.

In our study, high level of MDSC and low levels of CD4 T cells, NK cells and γδ T cells were found in the TME of high-risk patients. The abundance of NK cells predicted better outcomes in DLBCL patients, which may be attributed to the fact that high NK cell count enhances the efficacy of R-CHOP [37]. Studies have shown that MDSCs suppress the immune response to promote the occurrence and development of tumors in tumor microenvironment [38]. For example, a reduction in the number of MDSCs in patients with metastatic breast cancer treated with the drug cabozantinib was related to improved progression-free survival [39]. Recent evidence also has indicated that the presence of activated CD4 T cells in tumor tissue is associated with a better prognosis [40]. Besides, γδ T cells showed synergistic anti-tumor effects with activated αβ T cells and NK cells which improved patient outcomes [41, 42].

Tumor immune escape is considered as one of vital mechanisms in tumor occurrence and progression, and one of its main factors is the regulation of immune checkpoint expression [43]. The therapy targeting immune checkpoints has been a hot direction in the current clinical research and is viewed as one of effective antitumor therapies. In our study, several important immune checkpoints were found over-expressed in the high-risk group, such as PDCD1 and CD274. CD274, also known as programmed cell death ligand 1 (PD-L1), is a ligand for the inhibitory receptor PDCD1/PD-1, which regulates the activation threshold of T cells and limit T cell effector responses. The interaction between PD-L1 and PDCD1/PD-1 is a way to reduce anti-tumor immunity and evade immune system damage, thereby promoting tumor survival. Blocking the PD-1/PD-L1 pathway can normalize anti-tumor responses, but PD-1 inhibitors are not recommended to treat unselected DLBCL patients, due to low expression of PD-1/PD-L1 in DLBCL. Our results revealed that the high-risk group had significantly higher expression levels of CD274 and PDCD1, which contributed to identifying DLBCL

patients who are susceptible to PD-1 inhibitors [44–46]. Our study also showed that expression of JAK1 and JAK2 in high-risk group was lower than that in the low-risk group. The downstream target protein STAT of the JAK family is an important cytokine activated transcription unit in the immune response. The sustained activation of STAT3 and STAT5 can increase tumor cell proliferation and disease progression, it would be therapeutic targets for enhancing anti-tumor immunity [47, 48]. Activated STAT3 can drive the dissemination of DLBCL [49]. Related drugs, such as Cerdulatinib, is a novel dual SYK/JAK kinase inhibitor and has broad anti-tumor activity in DLBCL [50]. Therefore, treatment of the JAK pathway may have better efficacy in the low-risk groups.

In addition, due to the relationship between high-risk score and poor prognosis, the correlation between chemotherapy resistance and risk score was further studied. We found that the IC50 of bortezomib, rapamycin, AZD6244 and BMS-536924 in the high-risk group were lower than those in the low-risk group, suggesting that the high-risk group was more sensitive to these drugs. Bortezomib is a proteasome inhibitor that acts on the NF-κB signaling pathway, which is increased in non-GCB DLBCL. Combining bortezomib with R-CHOP in the treatment of recurrent non-GCB DLBCL is better than that of GCB DLBCL, and can improve the prognosis of non-GCB DLBCL [51]. Rapamycin is an mTOR inhibitor that can enhance the cytotoxicity induced by rituximab. Combined use of rapamycin may improve the efficacy of DLBCL patients [52]. AZD6244, a MEK inhibitor, has been shown to downregulate ERK substrate related to DLBCL cells and induce cell apoptosis [53]. BMS-536924 is a dual IGF1R/IR kinase inhibitor that has been experimentally proven to inhibit acute myeloid leukemia (AML) proliferation and serve as a potential therapeutic target for AML [54]. In the low-risk group, the IC50 of ABT-263 and cisplatin were lower than that of the high-risk group, indicating that they were sensitive to it. ABT-263 is one of the inhibitors of the Bcl-2 family. Experiments have shown that ABT-263 combined with a variety of chemotherapy drugs can inhibit and delay the growth of hematologic malignancies [55]. Cisplatin is a commonly used chemotherapy drug in hematological tumors. For patients with refractory relapse-resistant DLBCL who can tolerate high-dose chemotherapy, platinum-based regimen is the most commonly used, such as DHAP (dexamethasone, cisplatin and cytarabine) [56].

In our study, this scoring model was validated in both of the training dataset and the external validation set. When the nucleotide sequences of tumor samples from biopsies are confirmed and analyzed via Next Generation Sequencing of the same platform, the score can be calculated. Combining the above results of predicted chemotherapeutic sensitivity based on the scoring model, a new therapeutic strategy for DLBCL patients with different risk was formed, that is applying bortezomib, rapamycin, AZD6244 and BMS-536924 in the high-risk group, and cisplatin-containing regimens in the second-line treatment of relapse-refractory DLBCL patients in the low-risk group. Additionally, our study considered this scoring model as an indicator integrated in the constructed nomogram, and the subsequent DCA curves showed the positive net benefits of the constructed nomogram in guiding clinical decisions.

Nevertheless, there exist some limitations. Our study applied training dataset GSE10846 and validation dataset GSE87371 for the construction and verification of the scoring model. Although the detection platform is the same across both two datasets, the laboratories involved and their respective countries differ from each other. Therefore, differences in experimental operations (conducted by different individual experimenters), handling and exposure time of tumor samples prior to RNA extraction and inconsistent reagents occurs, causing discrepancies in our analysis.

Based on the above findings, we developed a TRGs-based scoring model for DLBCL, which represents a novel approach in this field. Our model has the potential to accurately predict the prognosis of DLBCL patients and facilitate the development of personalized treatment strategies.

Abbreviations

DLBCL: diffuse large B cell lymphoma; TRGs: telomere-related genes; K-M: Kaplan-Meier; COO: cell of origin; GCB: germinal center B-cell; ABC: activated B-cell; R-CHOP: rituximab plus cyclophosphamide, doxorubicin, vincristine, and prednisone; IPI: international prognostic index; RNA: ribonucleic acid; TERT: telomerase reverse transcriptase; TERC: telomerase RNA component; ALT: alternative length of telomeres; HL: hodgkin lymphoma; hTERT: human telomerase; TRGs: telomere-related genes; GEO: Gene Expression Omnibus; LASSO: least absolute shrinkage and selection operator; OS: overall survival; ROC: receiver operating characteristic; RT-qPCR: quantitative real-time PCR; ssGSEA: single-sample Gene Set Enrichment Analysis; DCs: dendritic cells; NK: natural killer; MDSCs: myeloid-derived suppressor cells; AUC: area under the curve; EBV: Epstein-Barr virus; NSCLC: non small-cell lung cancer; TME: tumor microenvironment; PD-L1: programmed cell death ligand 1; AML: acute myeloid leukemia.

AUTHOR CONTRIBUTIONS

Zhijia Zhao, Xiaochen Shen and Bo Tang performed the data analysis and interpreted the data. Jinhua Wang and Xiaochen Shen contributed to the experiments of this study. Siqi Zhao and Yuqin Tian prepared the draft. Siqi Zhao and Zhijia Zhao performed the visualization. Bo Tang and Xiaobo Wang revised the draft. Bo Tang and Xiaobo Wang designed the research and supervised all the work. All authors read and approved the final manuscript.

CONFLICTS OF INTEREST

The authors declare that the research was conducted in the absence of any commercial or financial relationships that could be construed as a potential conflict of interest.

ETHICAL STATEMENT AND CONSENT

The study was approved by the Ethics Committee of the Second Affiliated Hospital of Dalian Medical University. Informed consent was obtained from all subjects involved in the study.

FUNDING

The study was supported by the National Natural Science Foundation of China (81800203), Doctoral Startup Scientific Research Foundation of Liaoning Province (20180540088) and 1+X Program for Clinical Competency Enhancement-Improvement of MDT Project, the Second Affiliated Hospital of Dalian Medical University (2022MDTZY02).

REFERENCES

1. Alizadeh AA, Eisen MB, Davis RE, Ma C, Lossos IS, Rosenwald A, Boldrick JC, Sabet H, Tran T, Yu X, Powell JI, Yang L, Marti GE, et al. Distinct types of diffuse large B-cell lymphoma identified by gene expression profiling. Nature. 2000; 403:503–11. https://doi.org/10.1038/35000501 PMID:10676951

2. Ennishi D, Hsi ED, Steidl C, Scott DW. Toward a New Molecular Taxonomy of Diffuse Large B-cell Lymphoma. Cancer Discov. 2020; 10:1267–81. https://doi.org/10.1158/2159-8290.CD-20-0174 PMID:32616477

3. Patriarca A, Gaidano G. Investigational drugs for the treatment of diffuse large B-cell lymphoma. Expert Opin Investig Drugs. 2021; 30:25–38. https://doi.org/10.1080/13543784.2021.1855140 PMID:33295827

4. Miyawaki K, Kato K, Sugio T, Sasaki K, Miyoshi H, Semba Y, Kikushige Y, Mori Y, Kunisaki Y, Iwasaki H, Miyamoto T, Kuo FC, Aster JC, et al. A germinal center-associated microenvironmental signature reflects malignant phenotype and outcome of DLBCL. Blood Adv. 2022; 6:2388–402. https://doi.org/10.1182/bloodadvances.2021004618 PMID:34638128

5. Ilić I, Mitrović Z, Aurer I, Bašić-Kinda S, Radman I, Ajduković R, Labar B, Dotlić S, Nola M. Lack of prognostic significance of the germinal-center phenotype in diffuse large B-cell lymphoma patients treated with CHOP-like chemotherapy with and without rituximab. Int J Hematol. 2009; 90:74–80. https://doi.org/10.1007/s12185-009-0353-y PMID:19495929

6. Nyman H, Adde M, Karjalainen-Lindsberg ML, Taskinen M, Berglund M, Amini RM, Blomqvist C, Enblad G, Leppä S. Prognostic impact of immunohistochemically defined germinal center phenotype in diffuse large B-cell lymphoma patients treated with immunochemotherapy. Blood. 2007; 109:4930–5. https://doi.org/10.1182/blood-2006-09-047068 PMID:17299093

7. He MY, Kridel R. Treatment resistance in diffuse large B-cell lymphoma. Leukemia. 2021; 35:2151–65. https://doi.org/10.1038/s41375-021-01285-3 PMID:34017074

8. International Non-Hodgkin's Lymphoma Prognostic Factors Project. A predictive model for aggressive non-Hodgkin's lymphoma. N Engl J Med. 1993; 329:987–94. https://doi.org/10.1056/NEJM199309303291402 PMID:8141877

9. Blackburn EH, Greider CW, Szostak JW. Telomeres and telomerase: the path from maize, Tetrahymena and yeast to human cancer and aging. Nat Med. 2006; 12:1133–8. https://doi.org/10.1038/nm1006-1133 PMID:17024208

10. Ghanim GE, Fountain AJ, van Roon AM, Rangan R, Das R, Collins K, Nguyen THD. Structure of human telomerase holoenzyme with bound telomeric DNA. Nature. 2021; 593:449–53. https://doi.org/10.1038/s41586-021-03415-4 PMID:33883742

11. M'kacher R, Cuceu C, Al Jawhari M, Morat L, Frenzel M, Shim G, Lenain A, Hempel WM, Junker S, Girinsky T, Colicchio B, Dieterlen A, Heidingsfelder L, et al. The Transition between Telomerase and ALT Mechanisms in Hodgkin Lymphoma and Its Predictive Value in Clinical Outcomes. Cancers (Basel). 2018; 10:169.

https://doi.org/10.3390/cancers10060169
PMID:29848986

12. Shay JW, Wright WE. Telomeres and telomerase: three decades of progress. Nat Rev Genet. 2019; 20:299–309.
https://doi.org/10.1038/s41576-019-0099-1
PMID:30760854

13. Lima MF, Freitas MO, Hamedani MK, Rangel-Pozzo A, Zhu XD, Mai S. Consecutive Inhibition of Telomerase and Alternative Lengthening Pathway Promotes Hodgkin's Lymphoma Cell Death. Biomedicines. 2022; 10:2299.
https://doi.org/10.3390/biomedicines10092299
PMID:36140400

14. Gao J, Pickett HA. Targeting telomeres: advances in telomere maintenance mechanism-specific cancer therapies. Nat Rev Cancer. 2022; 22:515–32.
https://doi.org/10.1038/s41568-022-00490-1
PMID:35790854

15. Braun DM, Chung I, Kepper N, Deeg KI, Rippe K. TelNet - a database for human and yeast genes involved in telomere maintenance. BMC Genet. 2018; 19:32.
https://doi.org/10.1186/s12863-018-0617-8
PMID:29776332

16. Miyagishima S, Mani H, Sato Y, Inoue T, Asaka T, Kozuka N. Developmental changes in straight gait in childhood. PLoS One. 2023; 18:e0281037.
https://doi.org/10.1371/journal.pone.0281037
PMID:36758023

17. Li C, Zhao Q, Zhao Z, Liu Q, Ma W. The association between tropical cyclones and dengue fever in the Pearl River Delta, China during 2013-2018: A time-stratified case-crossover study. PLoS Negl Trop Dis. 2021; 15:e0009776.
https://doi.org/10.1371/journal.pntd.0009776
PMID:34499666

18. DeLong ER, DeLong DM, Clarke-Pearson DL. Comparing the areas under two or more correlated receiver operating characteristic curves: a nonparametric approach. Biometrics. 1988; 44:837–45.
PMID:3203132

19. Davison GM. Telomeres and telomerase in leukaemia and lymphoma. Transfus Apher Sci. 2007; 37:43–7.
https://doi.org/10.1016/j.transci.2007.04.006
PMID:17766184

20. Bandera Merchan B, Tinahones FJ, Macías-González M. Commonalities in the Association between PPARG and Vitamin D Related with Obesity and Carcinogenesis. PPAR Res. 2016; 2016:2308249.
https://doi.org/10.1155/2016/2308249
PMID:27579030

21. Hernandez-Quiles M, Broekema MF, Kalkhoven E. PPARgamma in Metabolism, Immunity, and Cancer: Unified and Diverse Mechanisms of Action. Front Endocrinol (Lausanne). 2021; 12:624112.
https://doi.org/10.3389/fendo.2021.624112
PMID:33716977

22. Korpal M, Puyang X, Jeremy Wu Z, Seiler R, Furman C, Oo HZ, Seiler M, Irwin S, Subramanian V, Julie Joshi J, Wang CK, Rimkunas V, Tortora D, et al. Evasion of immunosurveillance by genomic alterations of PPARγ/RXRα in bladder cancer. Nat Commun. 2017; 8:103.
https://doi.org/10.1038/s41467-017-00147-w
PMID:28740126

23. Wang SS, Davis S, Cerhan JR, Hartge P, Severson RK, Cozen W, Lan Q, Welch R, Chanock SJ, Rothman N. Polymorphisms in oxidative stress genes and risk for non-Hodgkin lymphoma. Carcinogenesis. 2006; 27:1828–34.
https://doi.org/10.1093/carcin/bgl013
PMID:16543247

24. Kobayashi T, Lam PY, Jiang H, Bednarska K, Gloury R, Murigneux V, Tay J, Jacquelot N, Li R, Tuong ZK, Leggatt GR, Gandhi MK, Hill MM, et al. Increased lipid metabolism impairs NK cell function and mediates adaptation to the lymphoma environment. Blood. 2020; 136:3004–17.
https://doi.org/10.1182/blood.2020005602
PMID:32818230

25. Chabay P. Advances in the Pathogenesis of EBV-Associated Diffuse Large B Cell Lymphoma. Cancers (Basel). 2021; 13:2717.
https://doi.org/10.3390/cancers13112717
PMID:34072731

26. Dolcetti R, De Rossi A. Telomere/telomerase interplay in virus-driven and virus-independent lymphomagenesis: pathogenic and clinical implications. Med Res Rev. 2012; 32:233–53.
https://doi.org/10.1002/med.20211
PMID:20549676

27. Huang YC, Lin SJ, Lin KM, Chou YC, Lin CW, Yu SC, Chen CL, Shen TL, Chen CK, Lu J, Chen MR, Tsai CH. Regulation of EBV LMP1-triggered EphA4 downregulation in EBV-associated B lymphoma and its impact on patients' survival. Blood. 2016; 128:1578–89.
https://doi.org/10.1182/blood-2016-02-702530
PMID:27338098

28. van Doorn R, Dijkman R, Vermeer MH, Out-Luiting JJ, van der Raaij-Helmer EM, Willemze R, Tensen CP. Aberrant expression of the tyrosine kinase receptor EphA4 and the transcription factor twist in Sézary syndrome identified by gene expression analysis. Cancer Res. 2004; 64:5578–86.

https://doi.org/10.1158/0008-5472.CAN-04-1253
PMID:15313894

29. Gao S, Wang S, Zhao Z, Zhang C, Liu Z, Ye P, Xu Z, Yi B, Jiao K, Naik GA, Wei S, Rais-Bahrami S, Bae S, et al. TUBB4A interacts with MYH9 to protect the nucleus during cell migration and promotes prostate cancer via GSK3β/β-catenin signalling. Nat Commun. 2022; 13:2792.
https://doi.org/10.1038/s41467-022-30409-1
PMID:35589707

30. Yuan C, Yuan M, Chen M, Ouyang J, Tan W, Dai F, Yang D, Liu S, Zheng Y, Zhou C, Cheng Y. Prognostic Implication of a Novel Metabolism-Related Gene Signature in Hepatocellular Carcinoma. Front Oncol. 2021; 11:666199.
https://doi.org/10.3389/fonc.2021.666199
PMID:34150630

31. Rattan R, Narita K, Chien J, Maguire JL, Shridhar R, Giri S, Shridhar V. TCEAL7, a putative tumor suppressor gene, negatively regulates NF-kappaB pathway. Oncogene. 2010; 29:1362–73.
https://doi.org/10.1038/onc.2009.431
PMID:19966855

32. Lafferty-Whyte K, Bilsland A, Hoare SF, Burns S, Zaffaroni N, Cairney CJ, Keith WN. TCEAL7 inhibition of c-Myc activity in alternative lengthening of telomeres regulates hTERT expression. Neoplasia. 2010; 12:405–14.
https://doi.org/10.1593/neo.10180
PMID:20454512

33. Yan Y, Gauthier MA, Malik A, Fotiadou I, Ostrovski M, Dervovic D, Ghadban L, Tsai R, Gish G, Loganathan SK, Schramek D. The NOTCH-RIPK4-IRF6-ELOVL4 Axis Suppresses Squamous Cell Carcinoma. Cancers (Basel). 2023; 15:737.
https://doi.org/10.3390/cancers15030737
PMID:36765696

34. Rugolo F, Bazan NG, Calandria J, Jun B, Raschellà G, Melino G, Agostini M. The expression of ELOVL4, repressed by MYCN, defines neuroblastoma patients with good outcome. Oncogene. 2021; 40:5741–51.
https://doi.org/10.1038/s41388-021-01959-3
PMID:34333551

35. Xu W, Ding H, Zhang M, Liu L, Yin M, Weng Z, Xu C. The prognostic role of fatty acid metabolism-related genes in patients with gastric cancer. Transl Cancer Res. 2022; 11:3593–609.
https://doi.org/10.21037/tcr-22-761
PMID:36388036

36. Zhang B, Xu A, Wu D, Xia W, Li P, Wang E, Han R, Sun P, Zhou S, Wang R. ARL14 as a Prognostic Biomarker in Non-Small Cell Lung Cancer. J Inflamm Res. 2021; 14:6557–74.
https://doi.org/10.2147/JIR.S340119
PMID:34916816

37. Yang Z, Yu W. Clinical significance of circulating neutrophils and lymphocyte subsets in newly diagnosed patients with diffuse large B-cell lymphoma. Clin Exp Med. 2023; 23:815–822.
https://doi.org/10.1007/s10238-022-00867-4
PMID:35939174

38. Marvel D, Gabrilovich DI. Myeloid-derived suppressor cells in the tumor microenvironment: expect the unexpected. J Clin Invest. 2015; 125:3356–64.
https://doi.org/10.1172/JCI80005
PMID:26168215

39. Kargl J, Busch SE, Yang GH, Kim KH, Hanke ML, Metz HE, Hubbard JJ, Lee SM, Madtes DK, McIntosh MW, Houghton AM. Neutrophils dominate the immune cell composition in non-small cell lung cancer. Nat Commun. 2017; 8:14381.
https://doi.org/10.1038/ncomms14381
PMID:28146145

40. Speiser DE, Chijioke O, Schaeuble K, Münz C. $CD4^+$ T cells in cancer. Nat Cancer. 2023; 4:317–29.
https://doi.org/10.1038/s43018-023-00521-2
PMID:36894637

41. Silva-Santos B, Mensurado S, Coffelt SB. γδ T cells: pleiotropic immune effectors with therapeutic potential in cancer. Nat Rev Cancer. 2019; 19:392–404.
https://doi.org/10.1038/s41568-019-0153-5
PMID:31209264

42. Ma L, Feng Y, Zhou Z. A close look at current γδ T-cell immunotherapy. Front Immunol. 2023; 14:1140623.
https://doi.org/10.3389/fimmu.2023.1140623
PMID:37063836

43. Jiang X, Wang J, Deng X, Xiong F, Ge J, Xiang B, Wu X, Ma J, Zhou M, Li X, Li Y, Li G, Xiong W, et al. Role of the tumor microenvironment in PD-L1/PD-1-mediated tumor immune escape. Mol Cancer. 2019; 18:10.
https://doi.org/10.1186/s12943-018-0928-4
PMID:30646912

44. Gordon SR, Maute RL, Dulken BW, Hutter G, George BM, McCracken MN, Gupta R, Tsai JM, Sinha R, Corey D, Ring AM, Connolly AJ, Weissman IL. PD-1 expression by tumour-associated macrophages inhibits phagocytosis and tumour immunity. Nature. 2017; 545:495–9.
https://doi.org/10.1038/nature22396
PMID:28514441

45. Munir S, Lundsager MT, Jørgensen MA, Hansen M, Petersen TH, Bonefeld CM, Friese C, Met Ö, Straten PT, Andersen MH. Inflammation induced PD-L1-specific T cells. Cell Stress. 2019; 3:319–27. https://doi.org/10.15698/cst2019.10.201 PMID:31656949

46. Xie W, Medeiros LJ, Li S, Yin CC, Khoury JD, Xu J. PD-1/PD-L1 Pathway and Its Blockade in Patients with Classic Hodgkin Lymphoma and Non-Hodgkin Large-Cell Lymphomas. Curr Hematol Malig Rep. 2020; 15:372–81. https://doi.org/10.1007/s11899-020-00589-y PMID:32394185

47. Yu H, Pardoll D, Jove R. STATs in cancer inflammation and immunity: a leading role for STAT3. Nat Rev Cancer. 2009; 9:798–809. https://doi.org/10.1038/nrc2734 PMID:19851315

48. Rani A, Murphy JJ. STAT5 in Cancer and Immunity. J Interferon Cytokine Res. 2016; 36:226–37. https://doi.org/10.1089/jir.2015.0054 PMID:26716518

49. Pan YR, Chen CC, Chan YT, Wang HJ, Chien FT, Chen YL, Liu JL, Yang MH. STAT3-coordinated migration facilitates the dissemination of diffuse large B-cell lymphomas. Nat Commun. 2018; 9:3696. https://doi.org/10.1038/s41467-018-06134-z PMID:30209389

50. Ma J, Xing W, Coffey G, Dresser K, Lu K, Guo A, Raca G, Pandey A, Conley P, Yu H, Wang YL. Cerdulatinib, a novel dual SYK/JAK kinase inhibitor, has broad anti-tumor activity in both ABC and GCB types of diffuse large B cell lymphoma. Oncotarget. 2015; 6:43881–96. https://doi.org/10.18632/oncotarget.6316 PMID:26575169

51. Ruan J, Martin P, Furman RR, Lee SM, Cheung K, Vose JM, Lacasce A, Morrison J, Elstrom R, Ely S, Chadburn A, Cesarman E, Coleman M, Leonard JP. Bortezomib plus CHOP-rituximab for previously untreated diffuse large B-cell lymphoma and mantle cell lymphoma. J Clin Oncol. 2011; 29:690–7. https://doi.org/10.1200/JCO.2010.31.1142 PMID:21189393

52. Wanner K, Hipp S, Oelsner M, Ringshausen I, Bogner C, Peschel C, Decker T. Mammalian target of rapamycin inhibition induces cell cycle arrest in diffuse large B cell lymphoma (DLBCL) cells and sensitises DLBCL cells to rituximab. Br J Haematol. 2006; 134:475–84. https://doi.org/10.1111/j.1365-2141.2006.06210.x PMID:16856892

53. Bhalla S, Evens AM, Dai B, Prachand S, Gordon LI, Gartenhaus RB. The novel anti-MEK small molecule AZD6244 induces BIM-dependent and AKT-independent apoptosis in diffuse large B-cell lymphoma. Blood. 2011; 118:1052–61. https://doi.org/10.1182/blood-2011-03-340109 PMID:21628402

54. Wahner Hendrickson AE, Haluska P, Schneider PA, Loegering DA, Peterson KL, Attar R, Smith BD, Erlichman C, Gottardis M, Karp JE, Carboni JM, Kaufmann SH. Expression of insulin receptor isoform A and insulin-like growth factor-1 receptor in human acute myelogenous leukemia: effect of the dual-receptor inhibitor BMS-536924 in vitro. Cancer Res. 2009; 69:7635–43. https://doi.org/10.1158/0008-5472.CAN-09-0511 PMID:19789352

55. Ackler S, Mitten MJ, Foster K, Oleksijew A, Refici M, Tahir SK, Xiao Y, Tse C, Frost DJ, Fesik SW, Rosenberg SH, Elmore SW, Shoemaker AR. The Bcl-2 inhibitor ABT-263 enhances the response of multiple chemotherapeutic regimens in hematologic tumors in vivo. Cancer Chemother Pharmacol. 2010; 66:869–80. https://doi.org/10.1007/s00280-009-1232-1 PMID:20099064

56. Gisselbrecht C, Glass B, Mounier N, Singh Gill D, Linch DC, Trneny M, Bosly A, Ketterer N, Shpilberg O, Hagberg H, Ma D, Brière J, Moskowitz CH, Schmitz N. Salvage regimens with autologous transplantation for relapsed large B-cell lymphoma in the rituximab era. J Clin Oncol. 2010; 28:4184–90. https://doi.org/10.1200/JCO.2010.28.1618 PMID:20660832

SUPPLEMENTARY MATERIALS

Supplementary Figures

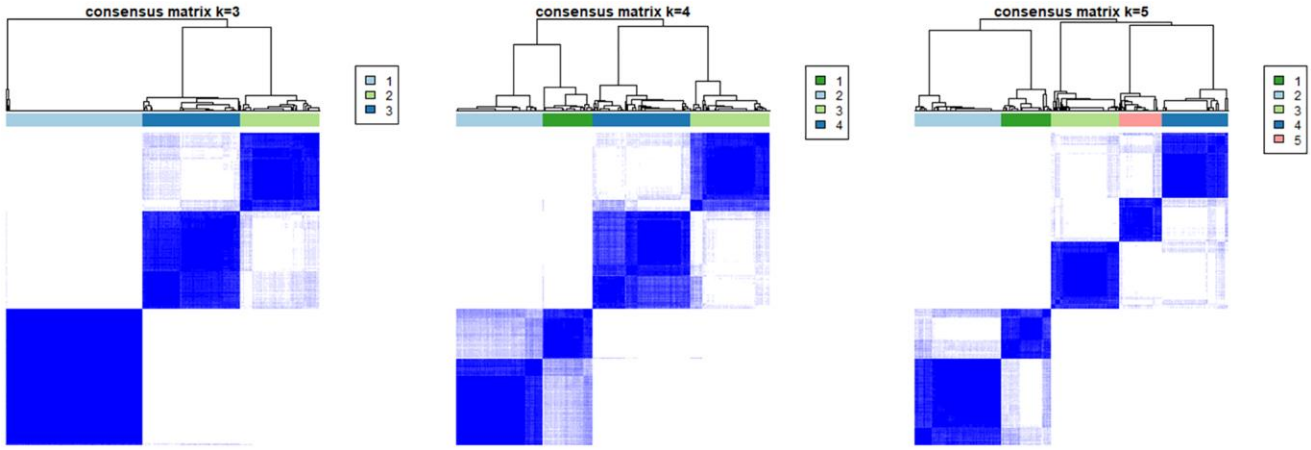

Supplementary Figure 1. The consensus matrix by cluster analysis based on TRGs. TRGs-based consensus clustering heatmap from 412 DLBCL samples of GSE10846 (k = 3–5).

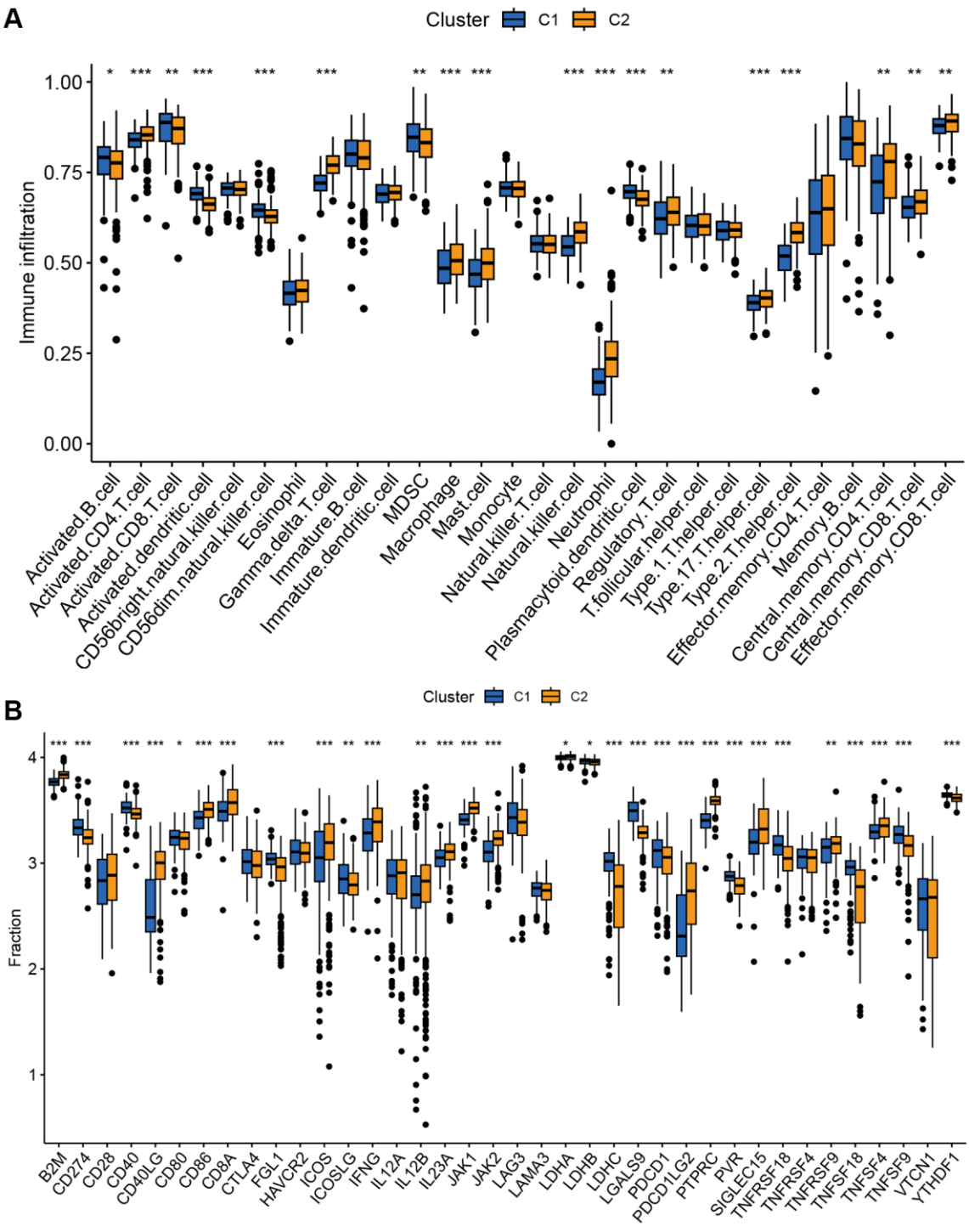

Supplementary Figure 2. Different immune profiles between two clusters. (**A**, **B**) The differences of (**A**) 28 immune cells and (**B**) 38 immune checkpoints between two clusters by ssGSEA ($^{*}p < 0.05$; $^{**}p < 0.01$; and $^{***}p < 0.001$).

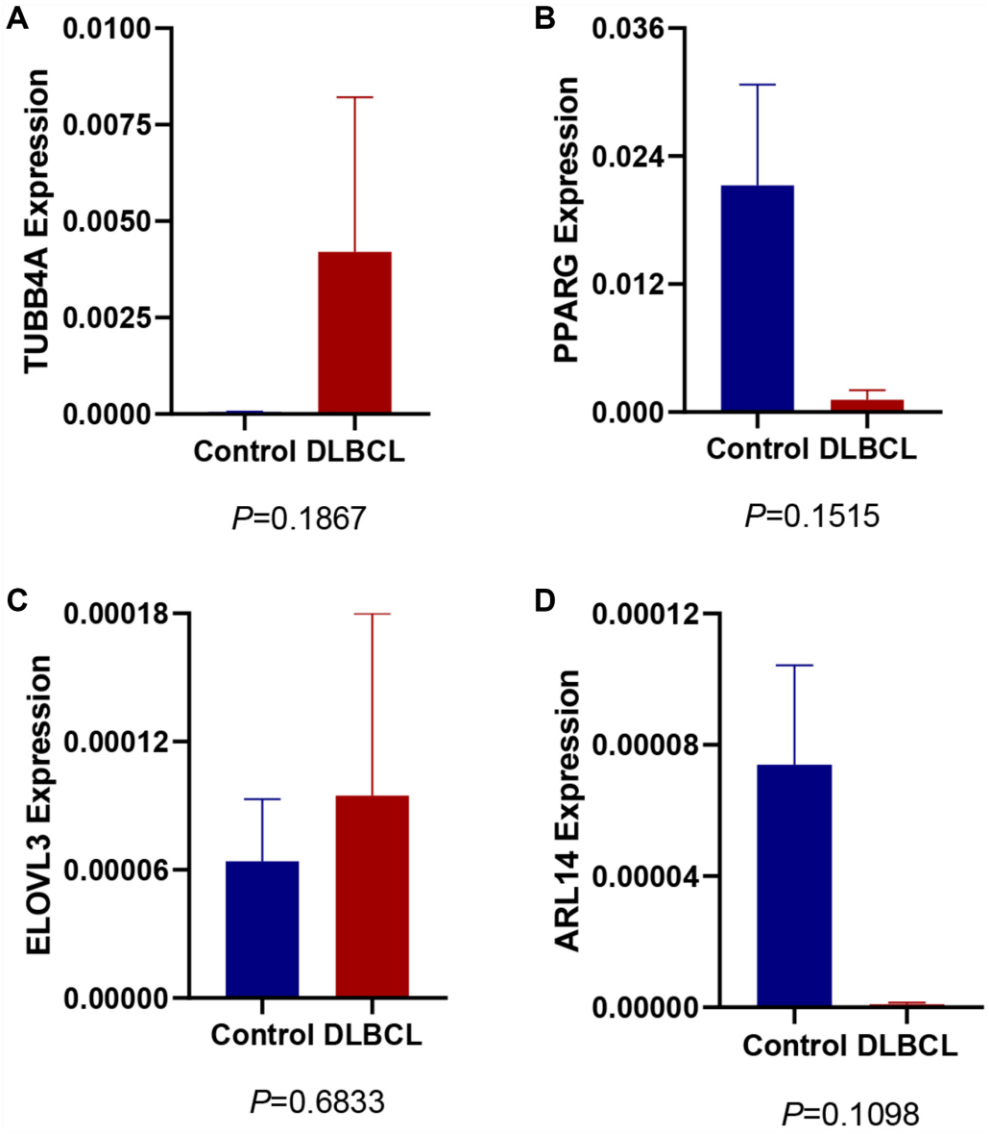

Supplementary Figure 3. Expression evaluation of other candidate TRGs in the model. (**A**–**D**) The expression of (**A**) TUBB4A (**B**) PPARG, (**C**) ELOVL3 and (**D**) ARL14 in DLBCL group and control group.

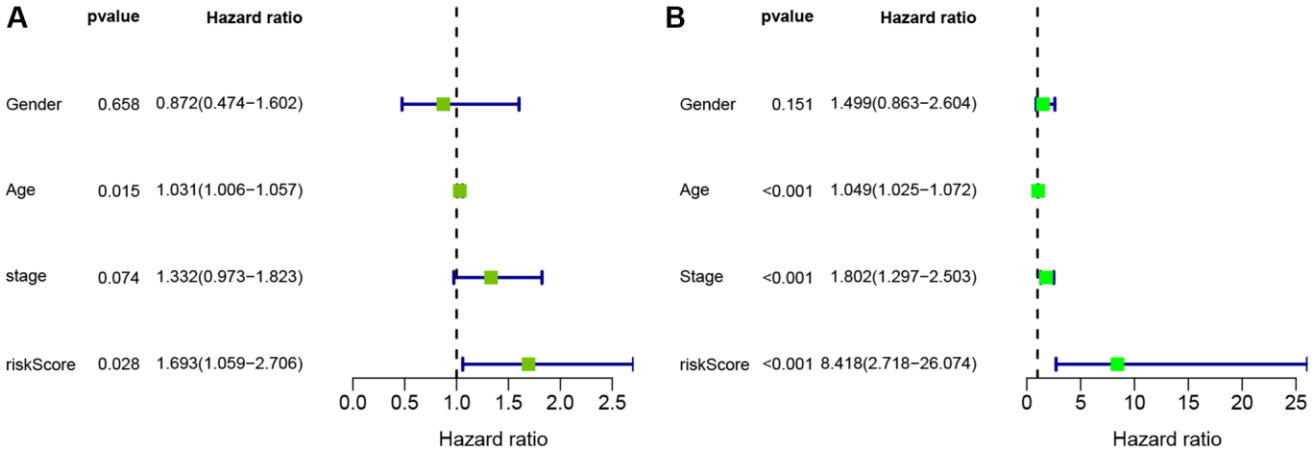

Supplementary Figure 4. Univariate Cox regression analysis of the TRGs score and clinical features. (**A**, **B**) Univariate Cox regression analysis of TRGs score and clinical features in (**A**) GSE10846 testing cohort and (**B**) GSE87371 cohort.

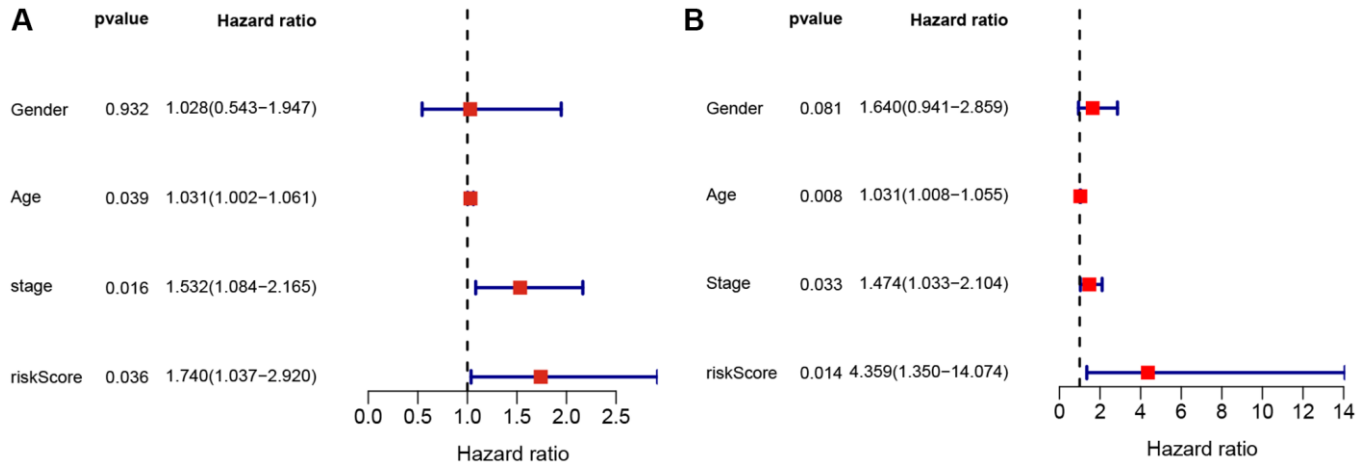

Supplementary Figure 5. Multivariate Cox regression analysis of the TRGs score and clinical features. (**A**, **B**) Multivariate Cox regression analysis of TRGs score and clinical features in (**A**) GSE10846 testing cohort and (**B**) GSE87371 cohort.

Supplementary Tables

Supplementary Table 1. The primer sequences of candidate genes and one reference gene (ACTB) for RT-PCR.

Primer	Sequence
TUBB4A Forward	5′–3′ CCGGACAACTTCGTGTTTGG
TUBB4A Reverse	5′–3′ TCGCGGATCTTACTGATGAGC
PPARG Forward	5′–3′ ACCAAAGTGCAATCAAAGTGGA
PPARG Reverse	5′–3′ ATGAGGGAGTTGGAAGGCTCT
ELOVL3 Forward	5′–3′ CTGTTCCAGCCCTATAACTTCG
ELOVL3 Reverse	5′–3′ GAATGAGGTTGCCCAATACTCC
TCEAL7 Forward	5′–3′ AAGGGAAGGAAGAGGTCCCAG
TCEAL7 Reverse	5′–3′ CTCTGTGCGGGGTAGTTTCC
EPHA4 Forward	5′–3′ TTCGCCCTATTTTCGTGTCTC
EPHA4 Reverse	5′–3′ TGGTAGGTTCGGATTGGTGTAT
ELOVL4 Forward	5′–3′ GAGCCGGGTAGTGTCCTAAAC
ELOVL4 Reverse	5′–3′ CACACGCTTATCTGCGATGG
ARL14 Forward	5′–3′ AAATCCGCAAACCAAACAAGC
ARL14 Reverse	5′–3′ TTCCAACTCGATCATTTCCACAT
ACTB Forward	5′–3′CCTGGCACCCAGCACAAT
ACTB Reverse	5′–3′GCCGATCCACACGGAGTA

Supplementary Table 2. Prognostic telomere-related genes.

ZSWIM7	THRAP3	RPS7	POLM	NCL	JSRP1	FANCB	CEP85	AHR
ZNHIT3	THOC6	RPS6KA5	POLE3	NCDN	JAZF1	FAM50A	CEP164	ACY1
ZNF703	THOC2	RPS4X	POLE2	NCBP2	JAK2	FAM175A	CENPO	ACTR5
ZNF414	THOC1	RPS28	POLDIP3	NCAPD3	IWS1	EZH1	CEBPA	ACTR3
ZNF281	THEMIS2	RPS17	POLD4	NBN	IVD	EXOSC6	CDKN2B	ACTR2
ZNF148	TFPT	RPS16	POLD2	NAT16	ITGAX	EXO1	CDK9	ACTN1
ZNF140	TFEC	RPS15A	POLD1	NAT10	ISCA2	ETAA1	CDK19	ACLY
ZMYM2	TERT	RPS14	POC1A	NASP	IRS4	ESRRA	CDK18	ABCF1
ZMIZ2	TERF1	RPN1	PNPO	NAGS	IRAK1	ESR2	CDK16	ABCC5
ZGPAT	TENM3	RPLP2	PNKP	NADK	IPO13	ERMP1	CDK13	ABCC4
ZCCHC7	TELO2	RPLP1	PNKD	NACA	IP6K3	ERH	CDK12	ABCC12
ZC3H18	TEAD1	RPL31	PMS1	MZF1	INO80E	ERCC5	CDK10	ABCC10
ZBTB9	TDRD7	RPL26L1	PLOD2	MYOM2	INO80C	ERCC4	CDCA8	ABCC1
ZBTB48	TCOF1	RPL19	PLK1	MYO10	INO80	ERCC3	CDC73	ABCB7
ZBTB44	TCF7L2	RPAP3	PLCL1	MYH9	ILF3	ERCC2	CDC45	AARS2
YY1	TCF7	RPAP1	PLCD1	MYH10	ILF2	EPS8L1	CDC37	AARS
YWHAQ	TCEAL7	RPAIN	PLCB4	MYC	IFRD2	EPHX2	CDC27	
YWHAG	TBCA	RPA3	PLCB3	MVK	IDH3A	EPHA4	CDC25B	
YWHAE	TBC1D15	RPA2	PLCB2	MUTYH	HYOU1	ENAH	CDC16	
YWHAB	TARDBP	RNF40	PLAT	MTF2	HUS1	EME1	CCT4	
YTHDF3	TALDO1	RINT1	PKMYT1	MTA1	HSPA4	EMD	CCNL2	
YTHDF1	TAF2	RGS3	PKM	MT1X	HSP90AB1	ELOVL6	CCNL1	
YRDC	TAF15	RFWD2	PKLR	MSN	HSP90AA1	ELOVL4	CCNE1	
YBX3	TADA1	RFPL3	PKIB	MRTO4	HOXA7	ELOVL3	CCNC	
XRCC6	SYNE2	RFC4	PITRM1	MRPS11	HNRNPM	ELAVL1	CCDC9	
XRCC4	SYAP1	REST	PIR	MRPL49	HNRNPA2B1	EIF5A2	CCDC155	
XRCC3	SUPT5H	REM2	PIN1	MPZL1	HNRNPA1	EIF4H	CCDC137	
XPO1	SUMO1	RELA	PIM2	MMS19	HNMT	EIF4A3	CBX5	
XBP1	SULT1C2	REL	PIK3CG	MLH1	HMGN2	EID3	CBX3	
XAGE2	SUDS3	REEP5	PIK3CD	MITF	HMGB1	EGR1	CASK	
WT1	STUB1	RECQL4	PIK3CB	MIS18BP1	HMGA1	EFCAB7	CARM1	
WRNIP1	STRADA	RECQL	PIK3C2A	MED13L	HMBOX1	EEFSEC	CAND1	
WRAP53	STOML2	RBX1	PIGK	MED13	HIST1H4I	EDC3	CAMK2G	

WDR5B	STIP1	RBM8A	PIF1	MED12L	HIST1H3G	E2F4	CAMK1D
WDR5	STAG2	RBM15B	PIAS1	MECOM	HIST1H3F	E2F1	CAMK1
WDR4	SSRP1	RBM14	PHYKPL	MDN1	HIST1H3B	DUSP10	CALML5
VPS18	SSB	RBL2	PHYHD1	MDH1	HIST1H1A	DST	CALD1
VGLL4	SRRM2	RBFA	PHLPP2	MDC1	HIF1A	DPYSL3	CACYBP
VDR	SRP14	RBBP9	PHLPP1	MCRS1	HHAT	DPY30	CABP4
VCP	SRM	RBBP7	PHF1	MCM7	HELZ	DOT1L	C20orf27
VAMP8	SPHK2	RB1CC1	PGS1	MCM5	HDGF	DOLPP1	C1D
VAMP4	SPA17	RAVER1	PGM2	MCM4	HDAC9	DNPH1	C19orf66
VAMP3	SORL1	RARRES2	PGD	MCM3AP	HDAC4	DNMT3B	BZW1
VAMP2	SOAT1	RAD9A	PFKP	MCM3	HDAC3	DNMT1	BRMS1
USP9X	SNRNP70	RAD54L	PEBP1	MCM2	HDAC1	DNAJC8	BRIP1
USP33	SNRNP40	RAD51D	PDS5B	MBD2	HAT1	DNAJC3	BRD2
USP21	SNF8	RAD23B	PDS5A	MAZ	H2AFY2	DNAJC11	BRCA1
UROS	SND1	RAD21	PDK4	MAST1	GTF2A1	DNAJB11	BOD1L1
UPF3A	SMU1	RAD18	PDK3	MAPKAPK5	GSTZ1	DNA2	BMP2K
UPF2	SMG6	RAC1	PDK1	MAPK12	GSS	DMD	BET1L
UPF1	SMG5	RABIF	PDGFRA	MAP7	GSPT1	DIP2C	BDKRB2
UFSP2	SMC6	RABGEF1	PDAP1	MAP4K3	GRWD1	DHX9	BCL11A
UEVLD	SMC5	RAB9A	PCNT	MAP3K4	GRPEL1	DHX40	BAZ2A
UBXN2B	SMC3	RAB6A	PCNP	MAP3K2	GRHL2	DHX38	BARD1
UBTF	SMC1A	RAB5C	PCMT1	MAP2K7	GREM1	DHX37	ATXN2L
UBE2R2	SMARCC2	RAB1B	PCBP1	MALT1	GPS1	DHX34	ATRX
UBE2M	SMARCA2	PUS7	PAXIP1	MADD	GPATCH8	DHX33	ATR
UBE2I	SLX4IP	PURA	PAX5	LYPLA1	GNL3L	DHX16	ATP5F1
UBE2D3	SLTM	PTPN23	PASK	LSM8	GNL3	DHFR	ATP5B
UBE2B	SLC7A9	PTMS	PARP4	LRSAM1	GMIP	DEK	ATP2B1
UBE2A	SLC7A8	PTMA	PARP3	LRRC59	GMDS	DDX50	ATP1A1
UBA1	SLC7A5	PTGES3	PARL	LRRC25	GLI2	DDX24	ATN1
UAP1L1	SLC7A11	PSME3	PAPSS1	LRR1	GIGYF2	DDX1	ATG16L1
UAP1	SLC3A2	PSMD13	PAICS	LPIN2	GIGYF1	DDB1	ATF1
TWF2	SLC25A6	PSMD10	PAFAH1B3	LONP1	GFPT2	DCTN2	ATAD5
TUBE1	SLC25A5	PSMB5	PACSIN3	LIG4	GET4	DCK	ATAD2
TUBB4B	SLC25A36	PSMA2	PACSIN2	LIG3	GDAP1	DBN1	ASF1A
TUBB4A	SKP1	PSKH2	PA2G4	LIG1	GBE1	DBF4B	ARRDC4
TUBB3	SIRT6	PSAT1	OSBPL9	LGMN	GATA6	DAXX	ARRDC3
TUBB2B	SIRT3	PRPSAP2	ORC4	LGALSL	GATA5	DARS	ARPC5
TUBB	SIN3B	PRPS2	OR2H1	LGALS1	GATA4	CTNNA1	ARPC2
TTI1	SIGMAR1	PRPF4B	OGG1	LEMD3	GATA3	CTDP1	ARMC6
TTBK1	SH3BP1	PRPF4	OGFR	LEMD2	GAS2L1	CTBP1	ARL4A
TSPYL5	SFR1	PRPF31	NXNL1	LDHB	GANAB	CTAG2	ARL14
TSPYL4	SFPQ	PRMT5	NVL	LDHA	GAK	CSTF2	ARID4B
TSG101	SF3B4	PRMT2	NUP98	LCP2	FZR1	CSNK2B	ARID4A
TSEN54	SETDB1	PRMT1	NUDT18	LCK	FXN	CSNK2A1	ARID3B
TRPS1	SETD1B	PRKD3	NUDT14	LAGE3	FUS	CSNK1E	ARID3A
TRPC5	SETD1A	PRKD2	NT5DC2	KMT2D	FUBP1	CSE1L	ARID1A
TRIP13	SERPINH1	PRKCSH	NSMCE4A	KMT2C	FRAT2	CRYGS	ARHGDIA
TRIP10	SEPHS2	PRKCQ	NSMCE2	KMT2B	FPGS	CPSF6	ARHGAP42
TRIM28	SENP3	PRKCB	NSFL1C	KMT2A	FOXR1	CPSF4	ARHGAP27
TRIM23	SENP2	PRKAR2A	NRIP1	KLF6	FOXP1	CPNE3	ARF3
TPRKB	SENP1	PRDX3	NR2F2	KLF2	FOXO1	COCH	APPL1
TPR	SEC61A2	PPP6R3	NPM1	KLF17	FOXN2	CNST	APEX1
TP73	SEC61A1	PPP2R1B	NOP9	KLF12	FOXM1	CNPPD1	APEH
TP53RK	SEC24B	PPP2R1A	NOL12	KIF13B	FOXK2	CMTR1	APAF1
TP53BP1	SEC16A	PPP2CA	NOC4L	KIAA1429	FOXJ3	CLPB	AP2A2
TP53	SDHA	PPP1R7	NME4	KIAA0430	FOXF2	CLK3	ANXA4

TOP3B	SCLY	PPP1R1B	NIPSNAP1	KHSRP	FOSL1	CLIC3	ANKLE1
TOP1	SAE1	PPP1R10	NIPBL	KEAP1	FKBP8	CLIC1	ANGPT4
TOMM34	RUVBL2	PPM1G	NFX1	KDM6A	FKBP3	CLASRP	AMPH
TNPO2	RUVBL1	PPM1F	NFE2L3	KDM4B	FHL1	CIRBP	AMPD3
TNKS2	RUNX2	POT1	NFATC2	KDM4A	FES	CHTF18	AMPD2
TNIP2	RTN4	POR	NFATC1	KDM1A	FBXO22	CHN1	ALDH2
TMX1	RTN3	POLR2E	NFAT5	KCTD17	FBP1	CHMP2B	AKT1
TMPRSS13	RTF1	POLR1E	NELFB	KCNS3	FBL	CHEK2	AKR7A3
TMEM109	RTEL1	POLR1C	NEK7	KAT2B	FARSA	CHD8	AKAP8
TLN1	RRAS2	POLR1B	NEK6	KAT2A	FANCM	CGGBP1	AIMP2
TKT	RRAGA	POLR1A	NEK4	JUND	FANCG	CFL1	AIFM1

Supplementary Table 3. Collinearity analysis of seven variables (age, ECOG, LDH level, number of extranodal sites, stage, TRGs risk score and IPI score).

	VIF
Age	1.776
ECOG	1.683
Extranodal_sites	1.316
LDH	2.357
Stage	2.797
RiskScore	1.121
IPI	7.345

Supplementary Table 4. Correlation analysis of seven variables (age, ECOG, LDH level, number of extranodal sites, stage, TRGs risk score and IPI score).

		Age	ECOG	Extranodal sites	LDH	Stage	RiskScore	IPI
Age	Pearson Correlation	1	.155*	−.049	.009	−.030	.164*	.345**
	Sig. (2-tailed)		.026	.480	.902	.668	.019	.000
	N	206	206	206	206	206	206	206
ECOG	Pearson Correlation	.155*	1	.184**	.275**	.266**	.167*	.561**
	Sig. (2-tailed)	.026		.008	.000	.000	.017	.000
	N	206	206	206	206	206	206	206
Extranodal sites	Pearson Correlation	−.049	.184**	1	.103	.374**	−.030	.354**
	Sig. (2-tailed)	.480	.008		.139	.000	.672	.000
	N	206	206	206	206	206	206	206
LDH	Pearson Correlation	.009	.275**	.103	1	.422**	.156*	.658**
	Sig. (2-tailed)	.902	.000	.139		.000	.025	.000
	N	206	206	206	206	206	206	206
Stage	Pearson Correlation	−.030	.266**	.374**	.422**	1	.206**	.703**
	Sig. (2-tailed)	.668	.000	.000	.000		.003	.000
	N	206	206	206	206	206	206	206
RiskScore	Pearson Correlation	.164*	.167*	−.030	.156*	.206**	1	.285**
	Sig. (2-tailed)	.019	.017	.672	.025	.003		.000
	N	206	206	206	206	206	206	206
IPI	Pearson Correlation	.345**	.561**	.354**	.658**	.703**	.285**	1
	Sig. (2-tailed)	.000	.000	.000	.000	.000	.000	
	N	206	206	206	206	206	206	206

*$p < 0.05$; **$p < 0.01$; ***$p < 0.001$.